HASP Student Payload Application for 2021

Payload Title: Stratospheric Measurements of Charged and Neutral Radiation	
Institution: McMaster University	
Payload Class (Enter SMALL, or LARGE): SMALL	Submit Date: January 8, 2021

Project Abstract:
With the reignited interest in human space flight, there exists a demand for greater health monitoring of astronauts. The hostile radiation environment of space poses serious and complex risks to the health of astronauts during interplanetary missions. Current estimates of consequential adverse health effects remain highly imprecise due to uncertainties in radiation quality factors. For example, recent estimates of cancer risk projections for a typical Mars mission have associated uncertainties of 400-600% and existing space qualified radiation detectors lack the ability to accurately measure radiation quality factors. Specifically, the active monitoring of exposure to neutrons, a major radiation dose hazard, is inadequate. To address this challenge, we have developed the Charged & Neutral Particle Tissue Equivalent Proportional Counter (CNP-TEPC), a unique radiation dosimeter with the capability of separating radiation dose contributions from charged and neutral radiation. The tissue equivalence of the detection system enables the collection of meaningful data since the dosimeter behaves analogously to a human cell. This real time radiation measurement device satisfies all radiation monitoring requirements of manned missions to low Earth orbit and future manned missions into deep space. A balloon flight will allow for the characterization of the instrument in a near space environment and play a key role in our mission of classifying radiological hazards in space. With major mechanical, electrical, and firmware advancements made during the HASP 2017 and 2018 flight campaigns, a fully functioning CNP-TEPC instrument with the capability of transmitting spectral data has been developed.

Team Name: CNP-TEPC Team		Team or Project Website: https://mcmasterneudose.ca/
Student Leader Contact Information:		Faculty Advisor Contact Information:
Name:	Amy Ling	Dr. Andrei Hanu
Department:	Chemical Engineering	Physics
Mailing Address:	1280 Main Street West	1280 Main Street West
City, State, Zip code:	Hamilton, Ontario, Canada, L8S 4K1	Hamilton, Ontario, Canada, L8S 4K1
e-mail:	linga9@mcmaster.ca	hanua@mcmaster.ca
Office Telephone:	N/A	N/A
Mobile Telephone:	(416) 270-8748	(519) 708-3552

Flight Hazard Certification Checklist

NASA has identified several classes of material as hazardous to personnel and/or flight systems. This checklist identifies these documented risks. Applying flight groups are required to acknowledge if the payload will include any of the hazards included on the list below. Simply place an (x) in the appropriate field for each hazard classification. **Note:** Certain classifications are explicitly banned from HASP (grey filled items on table below) and the remaining hazards will require additional paperwork and certifications. If you intend to include one of the hazards, you must include detailed documentation in section 3.8 of the application as required by the HASP Call for Payloads.

This certification must be signed by both the team faculty advisor and the student team lead and included in your application immediately following the cover sheet form.

Hazardous Materials List		
Classification	**Included on Payload**	**Not Included on Payload**
RF transmitters		**X**
High Voltage	**X**	
Pyrotechnics		**X**
Lasers		**X**
Intentionally Dropped Components		**X**
Liquid Chemicals		**X**
Cryogenic Materials		**X**
Radioactive Material		**X**
Pressure Vessels	**X**	
Magnets		**X**
UV Light		**X**
Biological Samples		**X**
Li-ion Batteries		**X**
High intensity light source		**X**

Student Team Leader Signature:  Jan 08 2021

Faculty Advisor Signature:  Jan 8th, 2021

Stratospheric Measurements of Charged and Neutral Radiation - Part IV

Arielle Ainabe, Jordan Bierbrier, Connor Chandran, Michael Chen, Xingzhi Cheng, Alessia Dinardo, Amy Ling, Juliana Onesi, Nick Phan, Ricardo Polo, Graham Power, Travis Ratnaharn, Ayesha Siddiqi, Ruoyu Sun, Bobby Tang, Liam Taylor, Gabriel Teichman, Adam Tyedmers, Nicholas Vrzovski

Student Lead:
Amy Ling
McMaster University
Chemical and Biomedical Engineering
1280 Main Street West, Hamilton, Ontario, L8S 4K1, CANADA

Faculty & Industry Advisors:
Dr. Andrei R. Hanu (McMaster University) - hanua@mcmaster.ca
Dr. Soo-Hyun Byun (McMaster University) - soohyun@mcmaster.ca
Dr. Eric Johnston (Nuclear Innovation Institute) - eric.johnston@nii.ca

Table of Contents

Table of Figures

Table of Tables

1. Payload Description

1.1 Payload Scientific / Technical Background

Human exploration to interplanetary destinations such as the Moon and Mars, and anticipated missions to further planets will become true in an expectable future. However, the current radiobiology study based on terrestrial accelerator sources cannot accurately assess the biological effectiveness and stochastic risk upon astronauts in hostile and complicated radiation environments during deep space missions [1-3]. For example, the estimated uncertainties of the projected cancer risk for a typical Mars mission are about 400 to 600% sourced from the uncertainties in radiation quality factors [2]. In order to better understand the potential radiation-induced health risk, *in situ* measurements of space radiation lineal energy spectra are needed. With the measured lineal energy spectra, the quality factor can be updated to provide more realistic estimation of the radiation dose in outer space.

The quality factors relate to absorbed dose and vary with the unrestricted Linear Energy Transfer (LET) in water as defined [4], but restricted LET is a more practical approach. The Tissue-Equivalent Proportional Counter (TEPC) is a microdosimetric instrument made by tissue-equivalent plastic and filled with tissue-equivalent propane gas and can provide accurate real-time absorbed dose measurement in human tissue. The lineal energy spectra measured by the TEPC with centimeter-sized sensitive volume can be used as a good approximation of restricted LET. TEPCs have been used for the Space Shuttle and International Space Station (ISS) program to monitor the radiation dose absorbed by astronauts since 2000 [5]. The first generation cylindrical TEPC was replaced by a laminated spherical type TEPC which overcomes up to 22% underestimation of dose due to non-isotropic response [6]. The laminated spherical type TEPC alone responds to all kinds of ionizing radiation which causes technical difficulties in separating the neutron component and charged particle from the total dose. The dose from neutrons is important to study as secondary neutrons generated by charged particles contribute a large portion of the total dose equivalent [7,8]. The direct detection and measurements of neutron energy spectra is problematic due to intense charged particles field [8]. The limits of individual dose measurement of charged particles and neutral particles constrains the steps toward interplanetary manned mission.

The NEUtron DOSimetry & Exploration (NEUDOSE) CubeSat is a miniature satellite being developed at McMaster University which is planned to be launched into Low Earth Orbit (LEO) where it will make detailed measurements of the microdosimetric lineal energy spectra. The primary scientific payload, the Charged & Neutral Particle Tissue Equivalent Proportional Counter (CNP-TEPC), is a novel radiation dosimeter containing a spherical TEPC detector surrounded by plastic scintillator – the Anti-Coincidence Detector (ACD). With the on-board electronic coincidence techniques, CNP-TEPC can separately map the interactions of charged particles and neutrons in real time and measure [9]. Due to negligible shielding from the CubeSat, the lineal energy spectra measured by the CNP-TEPC reflects the situation experienced by astronauts during extra-vehicular activities [9].

1.1.1 Mission Statement

As the race of human exploration of space continues, so does the race to understand the health risks associated with extra-planetary radiation. The CNP-TEPC, upon integration with the rest of the NEUDOSE and launched via a SpaceX Falcon 9 in 2022, will orbit the Earth at an altitude of 400km for one year. The CNP-TEPC will provide insight to the quantities of charged and neutral particle ionizing radiation absorbed by human tissue upon analysis of the generated lineal energy spectrum.

1.1.2 Mission Background and Justification

The health threat towards astronauts is posed by the complex and dynamic radiation environment in space, which has a distinct spectral composition from naturally occurring radiation on Earth. The space radiation environment consists of a complex mixture of charged and neutral particle radiation. To accurately estimate the exposure, multiple radiation detection technology would be required. CNP-TEPC developed in this program will focus on the dosimetry in the mixed radiation field. However, a radiation environment that is similar to the one in space is extremely difficult and costly to replicate on Earth. The height of a high-altitude balloon such as HASP is around 36 km above sea level. In such an environment, our payload will fly higher than 99% of the atmosphere and it will be explored to a radiation level that is very similar to space.

The ionizing radiation in the LEO mainly comes from 3 different sources: (1) Galactic Cosmic Rays (GCRs), (2) Earth's Radiation Belts (ERBs), and (3) Solar Particles Events (SPEs). However, at HASP's altitude, sources are only primary and secondary galactic cosmic rays mixing with high energy neutrons. This is because the ERBs are too high to affect any object in the height of HASP and solar particle events are relatively rare to occur. [10] GCR in space are composed of 98% protons and heavier ions (87% protons, 12% alpha particles, 1% heavy ion) 2% electrons and positrons. At the balloon float altitudes, collisions of primary GCRs with nuclei in the upper atmosphere result in a shower of lighter hadronic particles including, but not limited to pions, muons, electrons, neutrinos, and neutrons, which is the secondary GCR spectrum. The flux of GCR depends on many factors including height and solar cycle but is generally lower compared with neutron flux in the same environment. Although the flux of primary GCRs is relatively small, their large kinetic energies and high ionization density result in the highest radiobiological damage. Flying in HASP is a chance to simulate the environment of space for the CNP-TECP.

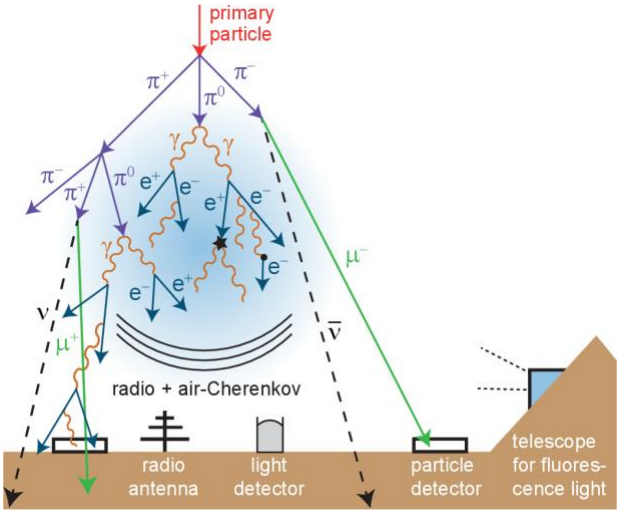

Figure 1: Cosmic ray air shower, collision of GCR with nucleus in the upper atmosphere [11]

Free neutrons that are outside of nuclei have a short mean lifetime of about 15 mins. Therefore, neutrons on or near-Earth come from within the solar system. At the balloon height, almost all

the neutrons come from the spallation reaction of GCR with nuclei of molecules in the upper atmosphere. As shown in Figure 2, the flux of neutrons in different heights of the atmosphere is lower than the flux of charged particles (mainly protons). Roughly 50% of the total ambient dose equivalent received is from neutrons [10, 12, 13]. From the radiobiological point of view, neutrons with energies between 0.1 to 2 MeV present the greatest risk as they can deeply penetrate the body, affecting blood-forming marrow in bones.

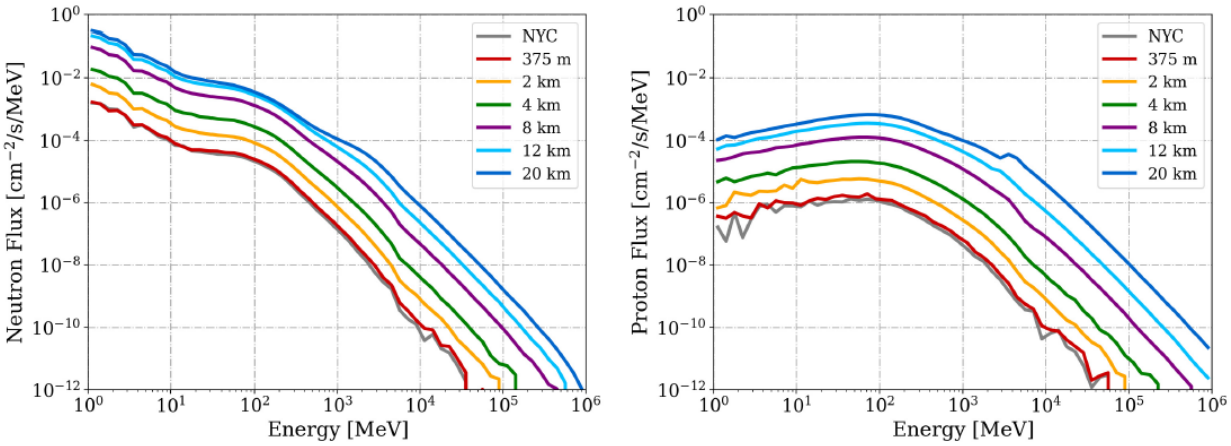

Figure 2: Neutron and proton flux in different height and energy [14]

From the EXPACS (EXcel-based Program for calculating Atmospheric Cosmic-ray Spectrum) database, the expected atmospheric neutron spectrum at HASP float altitude and latitude can be obtained. The spectrum consists of three large peaks centered on 0.1 eV, 1 MeV, and 100 MeV. The two lower energy peaks may come from the secondary neutron scattered by the lower atmosphere or the ground. The high energy peak, centered on 100 MeV, is a result of the primary, downward-going neutrons created by GCR spallation in the upper atmosphere. The production of atmospheric neutrons depends on incident GCR flux. Therefore, the neutron flux varies with geomagnetic cutoff, solar activity, and atmospheric depth. The neutron flux is much higher at balloon altitudes compared to sea level, also the 1 MeV peak neutrons in the spectrum have high radiobiological relevance.

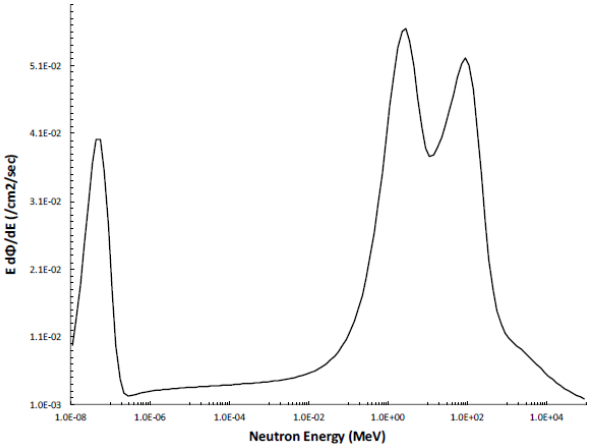

Figure 3: Atmospheric neutron spectrum at HASP altitude (36 km, 5.3 g cm−2) and latitude (34.5N, 104W) [15]

The overall radiation environment in the HASP float altitude is very similar to that in Low Earth Orbit (LEO) for both charged particles and neutrons. **With a flight on HASP, we will expose the CNP-TEPC to a relevant radiation environment, enabling us to characterize the instrument performance and determine the optimum instrument parameters for the future LEO flights.**

1.1.3 Mission Objectives

During HASP 2021, we propose to fly in the small payload category and further the progress of previous missions in preparation for our upcoming flight aboard NEUDOSE (www.mcmasterneudose.ca), a Canadian Space Agency funded CubeSat, in 2022. The mission objectives of HASP 2021 are to:

- Demonstrate stable operation of all CNP-TEPC subsystems in a near-space environment
- Validate the functionality of new revisions of the DAM and SiPM Module
- Measure variations in dose and quality factors of charged and neutral radiation
- Practice the full payload assembly procedure
- Validate thermal range functionality in TVAC
- Practice the solar panel assembly procedure
- Validate the solar panel assembly procedure (electrically)
- Testing/characterization of inhibit switches

1.2 Payload Systems and Principle of Operation

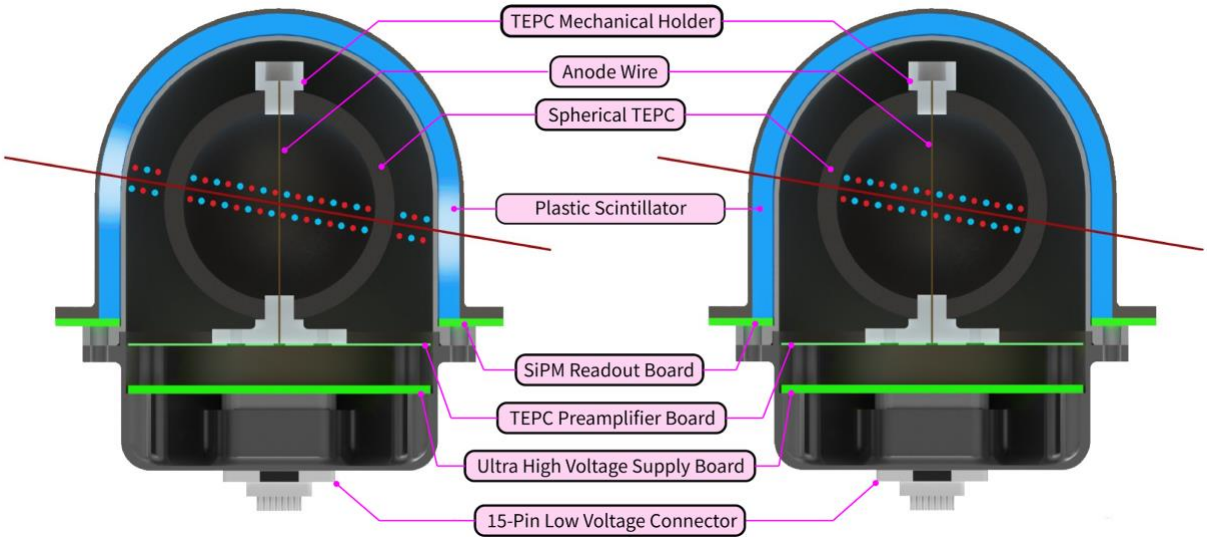

Figure 4: Cross section of the CNP-TEPC Instrument showing the difference between charged (left) and neutral (right) particle interactions with the detector.

The CNP-TEPC is an advanced radiation monitoring instrument developed to measure, in real time and for the first time, the microdosimetric spectra of charged particles and neutrons that could pose serious health threats to astronauts during future manned missions into deep space. The CNP-TEPC consists of two radiation detectors combined to enable real-time separation of absorbed dose and quality factors from charged particles and neutrons.

The inner radiation detector is the Tissue Equivalent Proportional Counter (TEPC). This component is composed of a sphere made of A-150 tissue-equivalent plastic with a gold anode traversing through the center held by two rexolite mounts. Since the TEPC is sensitive to all ionizing radiation, the measured lineal energy distribution often consists of a complex mixture of charged particle and neutral interactions which are difficult to separate. To separate the neutral

component of lineal energy from that produced by charged particles, the CNP-TEPC instrument implements an Anti-Coincidence Detector (ACD) that surrounds the spherical TEPC and provides a trigger signal whenever charged particles traverse it. The ACD features a polyvinyltoluene scintillator which, when traversed by ionizing radiation, emits light at a wavelength of 425nm. This light is detected by an array of 32 silicon photomultipliers (SiPMs) arranged at its base. This technique is often adopted in space borne gamma- or X-ray instruments to eliminate the charged particle background and is based on the fact that all charged particles traversing the spherical TEPC detector must also traverse the ACD. On the other hand, neutrons and other neutral particles will deposit their energy in either the TEPC or the ACD, but typically not both.

1.3 Major System Components

1.3.1 Tissue-Equivalent Proportional Counter (TEPC)

The TEPC consists of a dose cavity, a preamplifier module and a high voltage module (HVM). The dose cavity, the physical instrument for radiation measurement, has a wall that is made of electrically conductive A-150 tissue equivalent plastic and filled with low pressure (20–30 Torr) propane-based tissue equivalent gas (55% C_3H_8, 39.5% CO_2, and 5.5% N_2). When radiation interacts with the propane gas, the electron-ion pairs are formed and amplified via Townsend avalanches under the high voltage. The drifted electron-ion pairs induce charge on the anode wire to generate electronic signals which are integrated and read from a charge sensitive preamplifier. The microdosimetry relationship of the energy deposited ($\underline{\Delta\varepsilon}$) in a gas-filled centimeter-sized cavity (g) and the energy actually deposited in a micrometer-sized living cellular tissue (t) is:

$$\underline{\Delta\varepsilon} = \Delta x_g \left(\frac{\bar{s}}{\rho}\right)_g \rho_g = \Delta x_t \left(\frac{\bar{s}}{\rho}\right)_t \rho_t$$

where Δx is the distance that a particle travels, $\frac{s}{\rho}$ is the mass stopping power and $\rho$is the density. Since the gas in the cavity is tissue-equivalent, it provides the same electrical conductivity and radiation absorption as human adipose tissue, thus the TEPC can directly simulate the absorbed dose in human soft tissue at 2 µm depth and lineal energy spectrum of incident radiation up to 1,000 keV/µm [9].

The preamplifier module located below the TEPC is a PCB which contains an Amptek A250 preamplifier that is used to readout the TEPC signal. Based on calculation of a gas gain of ~1000 and W-value of the tissue-equivalent propane gas, the preamplifier was designed to be sensitive from 2.56 to 11.9 pC. The HVM sits behind the preamplifier module and it used to bias the TEPC. More information about the preamplifier module and HVM is available in Section 1.5.4. The radiation signals will be processed and communicated with the HASP flight computer via the Data Acquisition Module (DAM).

1.3.2 Detector Vessel

The components of the TEPC are housed in a detector vessel, which is composed of a vessel lid, a fill port, and a vessel base. The detector vessel provides a secured space for the TEPC and maintains the pressure of the tissue-equivalent gas at approximately 20-30 Torr. The detector

vessel lid is made of Aluminum 6061-T6 and the base is composed of AISI 304L stainless steel. The detector vessel is sealed with an Indium seal in addition to a laser welded bulkhead connector passing electrical signals and power to the components inside.

1.3.3 Anti-Coincidence Detector

The electronic coincidence is the key to differentiate the measured charged and neutron dose. To achieve this goal, a plastic scintillator coupled with a Silicon Photomultiplier (SiPM) array is designed as an Anti-Coincidence Detector (ACD). The ACD can separate neutron events from the mixed field of charge particles and neutrons based on the fact that charged particles are likely traversing the scintillator and also the TEPC, while neutral particles interact, typically, with only TEPC or scintillator. According to our GEANT4 Monte Carlo simulations results [9], for electrons with energy >10 MeV and protons with energy >100 MeV, the ACD achieves >0.995 coincidence detection efficiency; for neutrons with energy >1 MeV, 0.85 anti-coincidence detection efficiency can be achieved. The ADC system can efficiently discriminate charged particles from neutron events.

The plastic scintillator was chosen as the scintillator material and model EJ-200 from Eljen Technologies met the needed requirements that the scintillator need to be less sensitive to neutrons but maintain high sensitivity to charged particles. The scintillator was gently sanded using 600 grit sandpaper on all the surfaces except the base. And then 4 coats of Reflective Paint (EJ-510) were applied using a soft paintbrush with one-two hours of drying time in between coats. The temperature-dependent characteristic of the plastic scintillator requires temperature monitoring during the flight to ensure the scintillator works in a suitable range.
The scintillator emits ultraviolet light when ionizing radiation interacts with it. The scintillation photons then shall be incident on a circular SiPM array. Silicon-based PM can be integrated on a PCB and low bias voltage is required. The SiPM array contains 32 SensL MicroFJ-30035-TSV SiPMs. More information about SiPM arrays and related electronics can be found in Section 1.5.5.

The output signals from the SiPM array will be fed into the DAM and read by the CITIROC chip, an Application Specific Integrated Circuit (ASIC) developed by WeeROC. The CITIROC can handle signal readout for both energy and timing information. More information about CITIROC is described in Section 1.5.3.

1.3.4 Data Acquisition Module

The Data Acquisition Module (DAM) is the brain of the payload system consisting of the electrical hardwares and firmware required for the mission. The DAM is responsible for reading data from the CNP-TEPC, CITIROC and monitoring the status of several sensors throughout the data acquisition subassembly, communicating this data to the rest of the satellite. In addition to reading and communicating data, the DAM is also responsible for delivering power to each board and component involved in acquiring data from the CNP-TEPC. The DAM houses a Xilinx Spartan 6 Field-Programmable Gate Array (FPGA), responsible for the main data processing and communication from the CNP-TEPC, as well as the CITIROC ASIC, responsible for monitoring the outputs from the 32 SiPMs. The DAM also houses several power converters

responsible for providing power to all sections of the data acquisition subassembly. The DAM is connected through a single connector to receive power from the EPS sub-team, and communicate the data collected to the HASP flight computer. More details in electrical hardwares can be found in section 1.5.4. The firmware handles the control, data processing and external communication of the payload. It is implemented in the Spartan 6 FPGA with a MicroBlaze soft-core processor.

1.3.5 Power Distribution Module

The power distribution module (PDM) will accept and convert the power supplied by the HASP gondola to an acceptable voltage for the DAM and Electrical Power System (EPS) microcontroller. The PDM contains an EPS microcontroller, which will monitor the quality of power supplied through the EDAC connector by the use of ADCs.

1.3.6 Inhibit Switches

Four inhibit switches will be flown on the CNP-TEPC. They will be mechanically opened and electrically closed. The EPS microcontroller on the PDM will characterize these switches by recording the current through them as they hold a constant voltage. This data will be used to determine the performance of the switches ahead of our flight on the NEUDOSE CubeSat.

1.3.7 Solar Panels

Four solar panels, located on all X and Y faces, will be flown on our payload. However, they will not be used for the generation of power as we will be using the power supplied by the HASP gondola. Instead, they will be used to test the mounting process. This will provide an opportunity to practice mounting the solar panels before launch and identify any significant losses that may have resulted due to the mounting process.

1.4 Mechanical and Structural Design

The mechanical layout consists of 2 main assemblies: the CNP-TEPC instrument and the mounting structure that houses the CNP-TEPC and the Power Distribution Module (PDM) systems. Figure 9 below illustrates the location of the CNP-TEPC within the main structure and the main mechanical elements that make up the structural design.

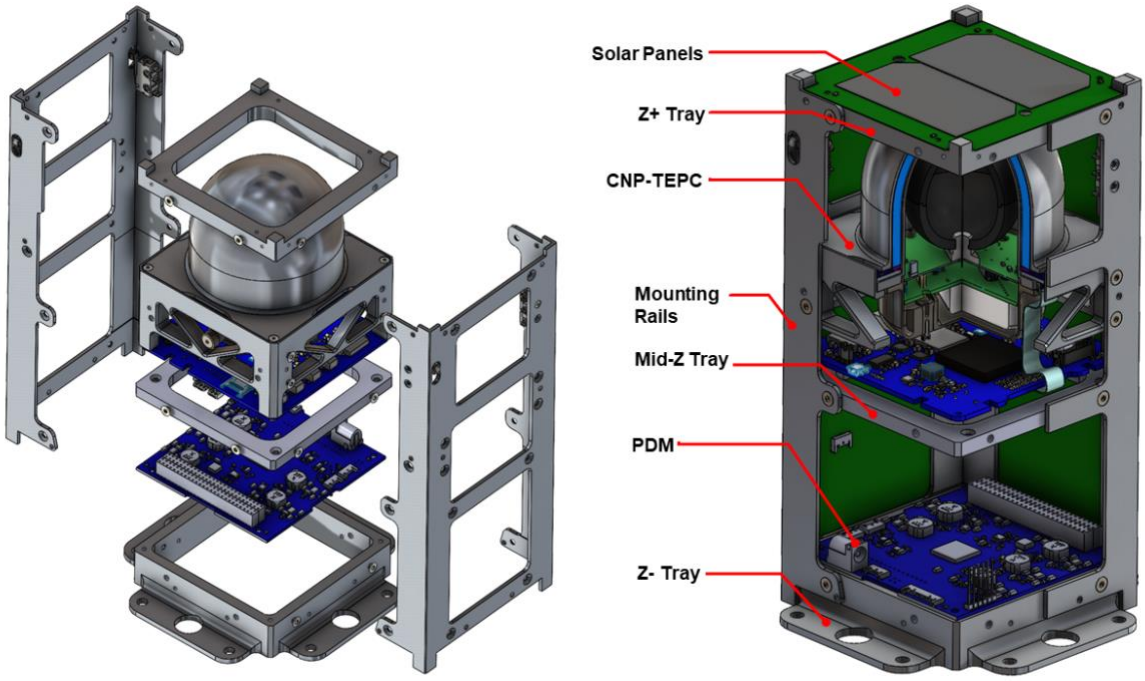

Figure 5: Payload components exploded (left) and assembled with cutaway (right). Some solar panels are not shown for clarity.

1.4.1 CNP-TEPC

The CNP-TEPC consists of two main detector components all held within a single instrument housing. The TEPC detector vessel contains the TE sphere, pre-amplifier and high voltage modules within a 304L stainless lower body and a 6061-T6 upper lid. The vessel is filled with a low-pressure tissue equivalent gas (20-30 torr) composed of 55% C3H8, 39.5% CO2, and 5.5% N2. The detector vessel is sealed using an indium O-ring seated in a triangular groove between the upper and lower detector vessel halves. Twelve M3x0.5 ISO 4762 screws along the periphery flange ensure even clamp loading of the indium O-ring. These screws thread into stainless steel coil wire helical inserts and are torqued to 75% of the fastener proof strength. Secondary locking of these fasteners is achieved with LOCTITE 242. A laser welded hermetic bulkhead micro-D connector allows signal and power to be passed to the components inside. A welded Swagelok fitting on the side of the vessel allows for a copper fill tube to be inserted and crimped after backfilling with a cold weld pinch off device, sealing the detector vessel.

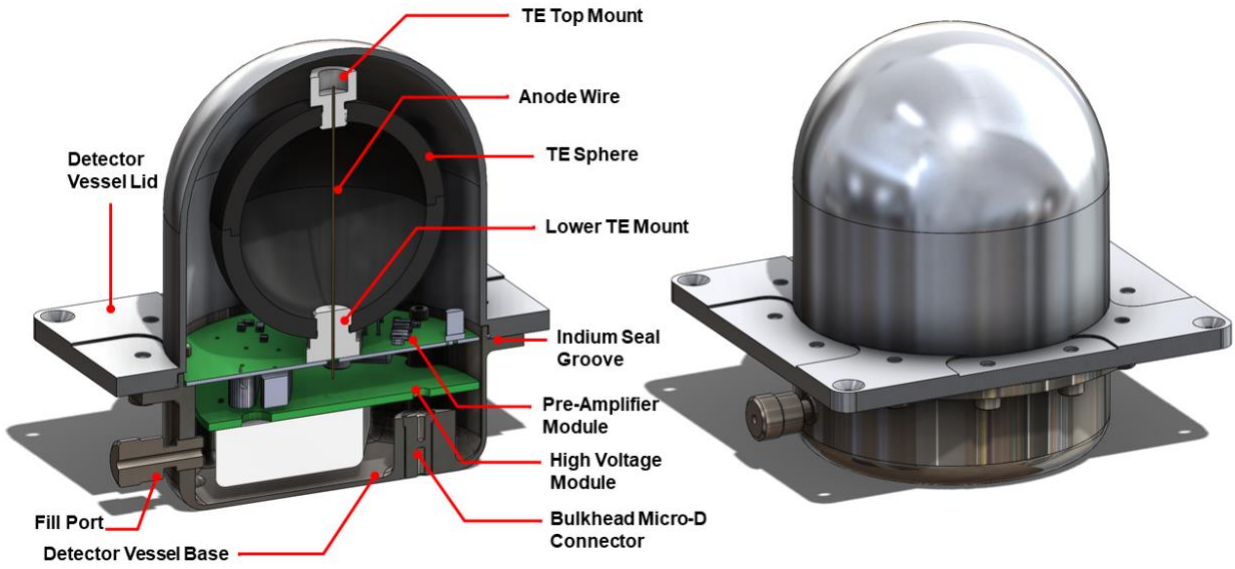

Figure 6: Breakdown of detector vessel components.

The detector vessel design, assembly and materials are almost identical to the detector flown in the payload during HASP 2017 and HASP 2018. Updates include helical inserts in the 12 flange holes to increase thread reliability in addition to a more robust Swagelok fill port as well as venting channels. This detector vessel design has undergone four TVac cycles from previous HASP missions in addition to prior lab bench testing and leak testing. Due to the low-pressure nature of the fill gas within the detector vessel it is in its highest stress state while on the ground in atmospheric conditions acting closer to a vacuum chamber. Structural analysis was performed assuming loading of a 104.8 kPa atmosphere and no detector fill pressure. This represents the highest static load on the vessel which occurs during initial backfilling and purging. These simulations indicate the detector vessel has a FOS of 3.26 due to static atmospheric loading and a minimum buckling load factor of 79 with conservative loading and assumptions. In LEO, with only an internal pressure of 40 torr, the safety margin is even higher with a FOS of 64. Further information on the detector vessel can be found in Appendix E.

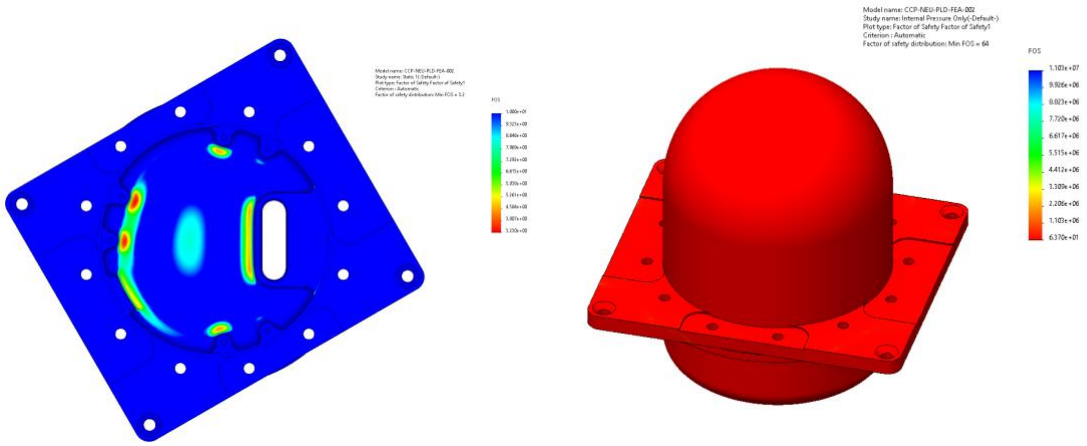

Figure 7: (Left) FEA analysis of detector vessel under atmospheric conditions and internal vacuum with a FOS of 3.26, (Right) detector vessel in vacuum environment with 40 torr internal pressure with a FOS of 64.

The ACD sits on top of the detector vessel and comprises the SiPM Module, the scintillator dome, a silicone optical interface and a domed lid that constrains the components. The lid is made from 6061-T6 and is fastened to the instrument housing with four M2.5 screws. This provides axial clamping on the scintillator and prevents radial movement of the ACD components.

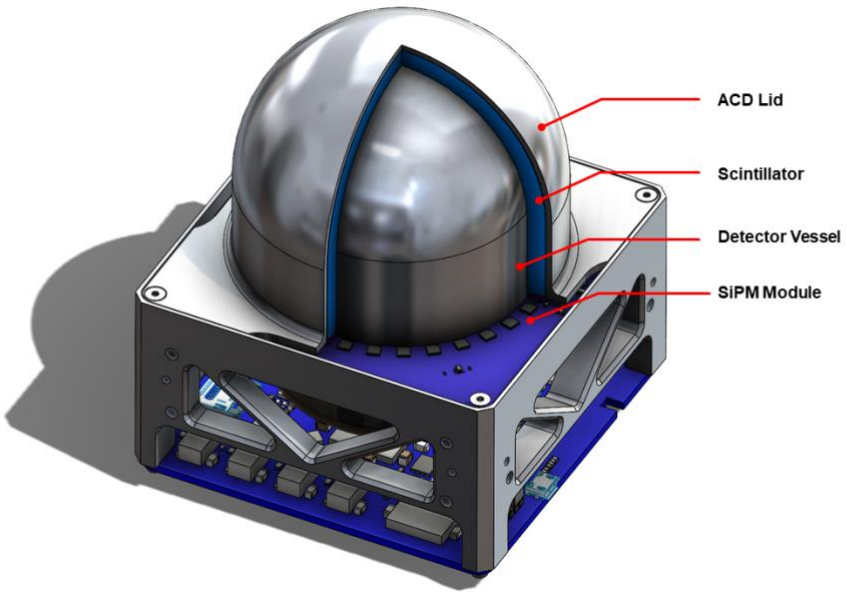

Figure 8: Breakdown of components making up the ACD.

The instrument housing provides mounting points for both the detector vessel as well as the ACD in addition to mounting locations to secure the entire instrument assembly to the structure rails. The data acquisition module is mounted to the bottom side of the instrument housing allowing access to all connectors for programming and debugging prior to flight. Vent channels have been placed throughout the instrument to avoid trapping atmospheric gases.

1.4.2 Mounting Structure

The structure of the 2021 HASP payload is similar to that of the previously flown mechanical structure by the team in 2018. The assembly is made up of two identical rails held together by three structural trays positioned along the length of the rails. The CNP-TEPC is secured to the rails between the top and mid tray using twelve M3x0.5 screws. All of the mounting structure components are machined from Al 6061-T6. Each tray is connected to the rails through the use of eight M3x0.5 ISO 10642 flat head screws. These fasteners thread into tapped holes in the trays with stainless steel coil wire inserts to reduce risk of fastener pullout. Primary fastener locking is achieved utilizing bolt preload with secondary locking provided by LOCTITE 242 threadlocker.

The rail, top and mid tray geometry are identical to those planned for the mission's anticipated launch date in 2022. This allows for four full length solar panels to be mounted to the sides of the structure, allowing for testing of the final flight configuration of the solar array. Additionally, the

CNP-TEPC assembly and structure geometry is almost identical to the 2022 mission's final flight configuration allowing for standardized assembly procedures to be developed and fine-tuned.

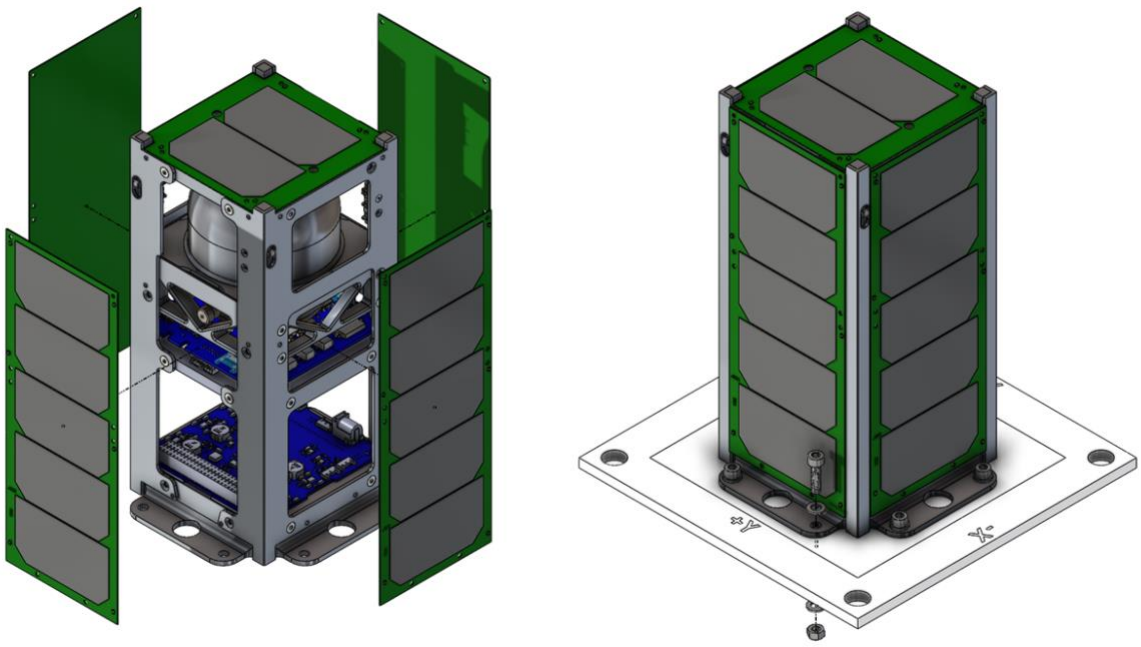

Figure 9: Solar panel configuration (left) and final payload mounted to interface plate (right).

The payload is secured onto the provided mounting plate by eight M5 bolt and nut assemblies. Locking of the bolts is accomplished by the use of nylon-insert lock nuts secured on the backside of HASP payload plate. Serial connection and EDAC harnesses will be fed through a cutout on the bottom of the HASP student interface plate and connect to the Z- face of the PDM.

To verify the mechanical stresses seen by the payload during launch, multiple FEA studies were conducted on the structure assembly. 5G and 10G shock simulations were conducted to analyze both stresses seen in the structure components as well as to verify no occurrences of bolt failure due to the prescribed loading. Analysis was conducted assuming bolted connections between components with no-penetration contact sets between components. The same final converged mesh was used in both 5G lateral and 10G vertical simulations.

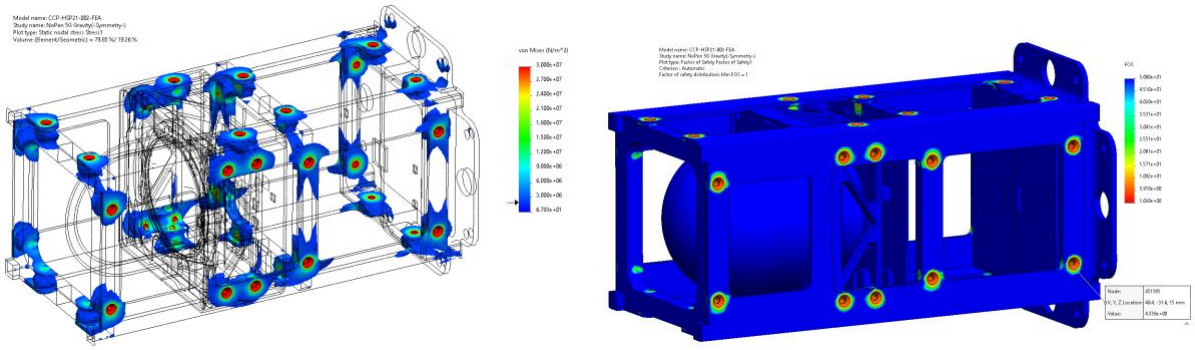

Figure 10: 5G lateral stress simulations. Von Mises Stress iso-clipped at 2MPa (right) FOS Plot with minimum structure FOS=4.5 (left).

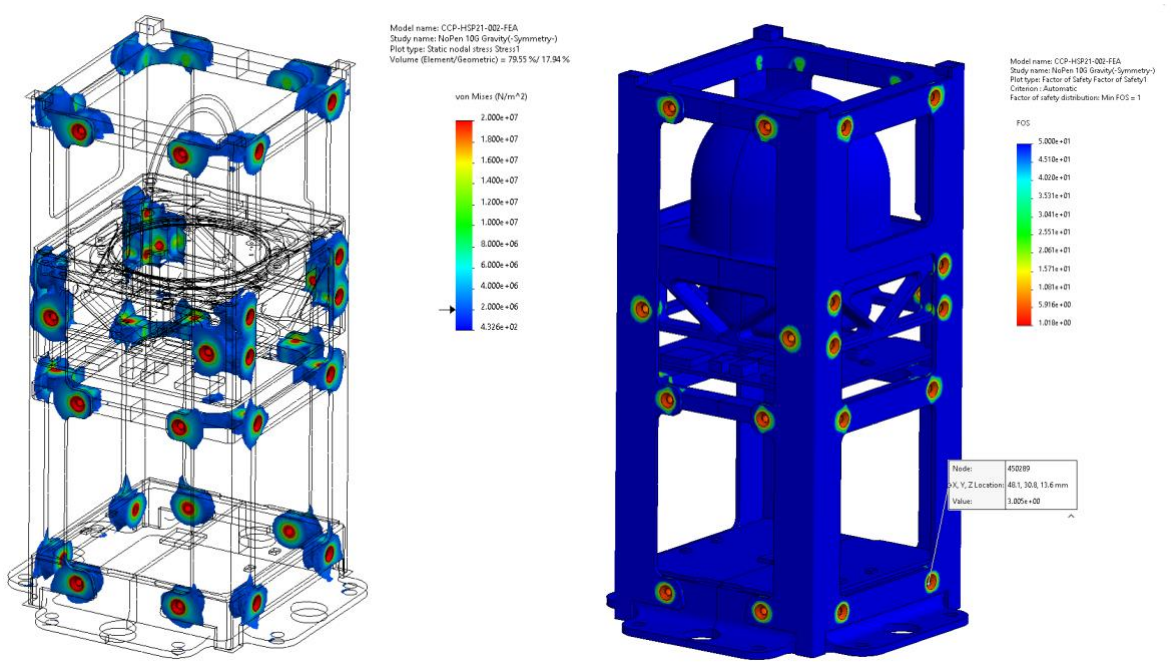

Figure 11: 10G vertical stress simulations. Von Mises Stress iso-clipped at 2MPa (right) FOS Plot with minimum structure FOS=3.0 (left).

In the above figures it can be seen that the minimum factor of safety on the structure based on simulation analysis is 3.0. These peak stresses are only seen within the bolt contact regions with the surrounding structure having a much greater factor of safety. These elevated stresses are due to both bolt pre-load as well as transferred stress from the 5G and 10G loads. Analysis of the forces seen by the bolts were tabulated and their individual safety factors calculated, with the lowest bolt FOS to be 4.9 with a Grade 10.9 fastener.

1.5 Electrical Design

The electrical design of the small payload is split into several different sections:

- Power Distribution Module (PDM)
- Solar Panels
- Data Acquisition Module (DAM)
- Tissue Equivalent Proportional Counter (TEPC) Electronics
- Silicon Photomultipliers (SiPM)

Each section describes a key component of the electrical architecture for the CNP-TEPC in detail.

1.5.1 Power Distribution Module (PDM)

Within the electrical design is the Power Distribution Module (PDM). Similar to HASP 2017 and 2018, the payload will be powered directly from the HASP bus using the PDM. The PDM is responsible for monitoring and filtering the power received from HASP, as well as converting the received power to an acceptable voltage for the DAM and Electrical Power System (EPS) microcontroller. A block diagram of the power flow and electrical distribution system can be found in Figure 12 below.

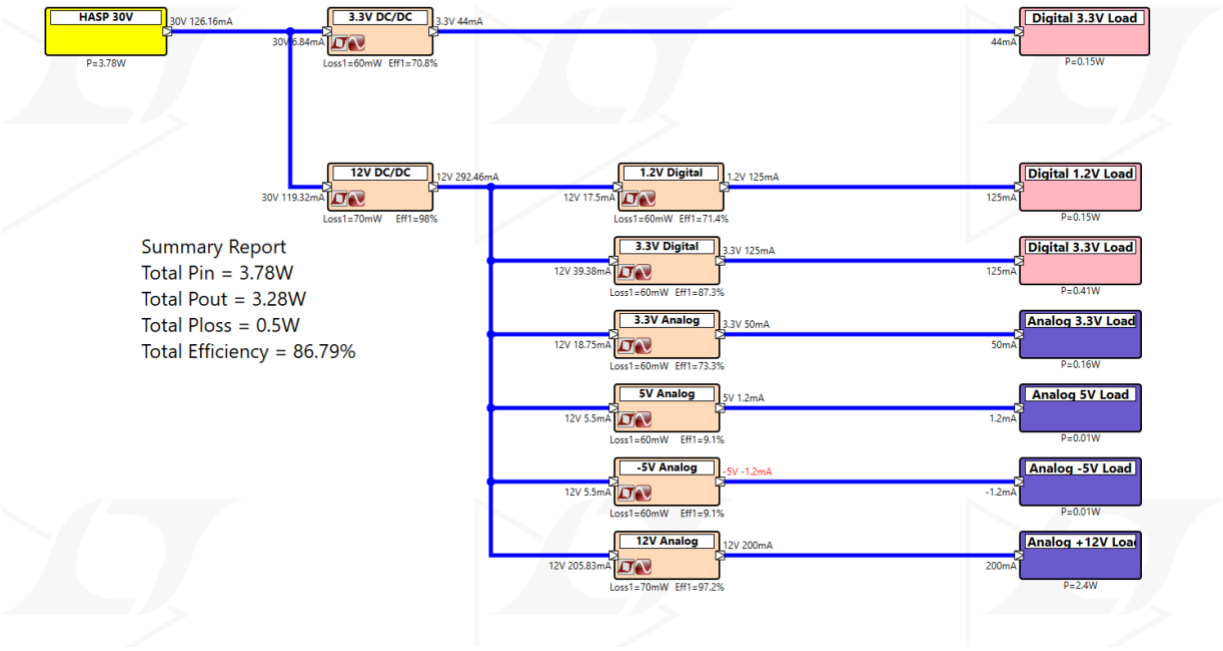

Figure 12: Block diagram of the power flow and electrical distribution system.

The PDM uses two high efficiency LT8610 regulators to step down the +30V to +12V and +3.3V required by the CNP-TEPC and Electrical Power System microcontroller. The +12V power for the CNP-TEPC is then further converted on the DAM, discussed in section 1.5.4.

The payload will interface with HASP similarly to how it was interfaced with in the previous HASP 2017 and 2018 missions. The pins from the EDAC connector that are to be used include the +30V power supply pins (A, B, C, D) and the ground pins (W, T, U, X). The DB9 connector will serve as the primary data port between the payload and HASP. The payload will utilize the Tx and Rx pins from the DB9 connector, grouping these two lines with the power and ground pins from the EDAC connector. Each of these lines will feed into a 6 pin T1SS Discrete Wire Cable (P/N T1SS-06-28-XX-08.0-X-XX). The four +30V wires will feed into two pins of the connector, with the four GND wires feeding into two different pins, with the Rx and Tx pins populating the last two pins. Each of the pins not in use will be capped off, labelled as no-connects.

Onboard the PDM is the EPS microcontroller, responsible for monitoring the quality of the power supplied from HASP, as well as storing test data from the mounted solar panels. The microcontroller will be using ADCs to monitor the voltage and current values from both the 3.3V and 12V power supplies, as well as monitor the voltage and current received from HASP. This monitoring system will also be used to characterize the inhibit switches. These switches will be mechanically opened and electrically closed. The switches will be characterized individually by holding a known voltage across them while the microcontroller logs the current through them. The data will then be stored using the on board flash memory which we can later analyze to see if they have misbehaved (electrically closed).

1.5.2 Solar Panels

Although we will be flying solar panels, they will not be used to generate power. Instead, their purpose is to test the efficacy of the mounting process. These panels will dissipate any generated power into a load resistor, which the PDM will be able to detect and measure using its on board circuitry. This data can be used to check against a set of theoretical values of what we would expect to see if there are any significant losses that may have occurred due to the mounting process.

This will also provide an extra opportunity for us to be able to practice the mounting of the cells, allowing ourselves to be further familiar with the process. The added conditions of needing them to survive TVac/flight will provide an avenue for us to self-evaluate and see what parts of the process can be improved.

1.5.3 Data Acquisition Module (DAM)

The data acquisition module (DAM) processes the output signals from the TEPC and ACD instruments, monitors the status of the CNP-TEPC through three ADCs, and communicates CNP-TEPC data via a CAN and RS232 bus connection. Since our last application in 2019 we have made changes to the DAM, with the largest change being the reduction of different components used throughout the DAM. The top and bottom of the DAM can be found in Figure 13 below.

DAM Power Architecture

The DAM houses 6 different power supplies to meet the power requirements for all components of the CNP-TEPC. The power supplies are separated into digital supplies (for digital components) and analog supplies (for analog components). The LTM4619 power converters are used to create the power for digital components for the CNP-TEPC. The LTM4619s produce 1.2V and 3.3V used for all digital components on the DAM (ADCs, Spartan 6 FPGA, Memory, etc.). The power requirements for the analog components are created from four LTM8045 converters that output 3.3V, 5V, -5V and 12V. Analog components include all components that are responsible for data acquisition, including components in the TEPC front end electronics, signal filtering and amplification, CITIROC analog components, and the High Voltage Power Supply. **Each of the analog power supplies**

are not powered by default when the payload is applied power. The analog converters need to be pulled up through an enable signal from the FPGA in order to be turned on.

All power converters on the DAM receive 12V from the PDM via a single connector. This 12V power is supplied by the PDM's own LT8610 power converters, converting the 30V from HASP.

The DAM interfaces with the PDM via a single 10 pin Molex connector. On this connector, there are:

- 2 pins for power
- 2 pins for GND
- 2 pins for CAN bus (One positive pin, one negative)
- 2 pins for RS232 communication (Rx and Tx)
- 2 pins unpopulated

For the HASP 2021 mission, the DAM will be utilizing the RS232 as the main form of communication between the payload and HASP. The RS232 Rx and Tx signals will originate on the DAM through the usage of a MAX3221 integrated circuit, with the signals transmitted through the PDM to the HASP DB9 connection.

Spartan 6 FPGA

The Spartan 6 FPGA is the main processor used on the DAM and is responsible for processing all acquired data, preparing it for transmission to the HASP flight computer, monitoring temperatures, currents, voltages and pressures, as well as controlling all other settings of the payload that are able to be modified. The Spartan 6 monitors and controls each of the electronic components involved in the CNP-TEPC through firmware developed specifically for data acquisition and monitoring. The uploaded firmware on the FPGA processes acquired data, controls specific instrument settings, as well as communicates all data through the use of several data handlers. The Spartan 6 is selected for this mission due to its proven tolerance to high levels of radiation as well as wide range of operating temperatures.

Citiroc

Another main component of the DAM is the CITIROC 1A, used specifically for controlling and reading out the acquired data from the SiPMs. The SiPMs connect to the DAM through a 50-pin ribbon cable, where they return analog photocurrent values. The CITIROC receives these photocurrents, digitizes them and sends them to the FPGA.

The CITIROC is split into both an analog section and digital section. The digital section of the CITIROC controls the threshold noise level, a threshold representing the difference between a particle interaction and regular noise for the SiPMs.

In order to monitor the status and output of the TEPC, the main functions of the DAM are to condition and digitize the small amplitude signals from the TEPC preamplifier, as well as provide temperature and pressure information for gas density calculations. The output of the charge sensitive preamplifier, which is housed inside the pressure vessel and near the TEPC, is used as input signal to a digital pulse processing circuit.

Housekeeping Analogue to Digital Converters (ADCs)

The housekeeping ADCs which are responsible for monitoring the voltage, current, temperature and pressure through the various sensors on the CNP-TEPC. There are three located on the DAM 8 pins each. They take the analogue inputs from the Spartan 6 FPGA, TEPC and SiPM bias voltage monitors, SiPM bias current monitor and the CITIROC and SIPM temperature sensors. These inputs are digitized and sent via SPI to the FPGA for processing.

1.5.4 Tissue Equivalent Proportional Counter (TEPC) Electronics

The TEPC is one of the two instruments on the payload used for detecting particle interactions on the satellite in addition to the Anti-Coincidence Detector. The TEPC is made up of tissue equivalent plastic filled with a tissue equivalent propane gas. The TEPC has an anode wire held at ground potential running through the centre of it, with the spherical tissue equivalent plastic biased to create an electromagnetic field within the instrument in order to determine the amount of charge deposited in each particle interaction. More information about the TEPC can be found in section 1.3.

Two of the major electric components involved with the TEPC are the High Voltage Module (HVM) and the TEPC Front End Electronics (FEE), each of which are discussed in detail below.

TEPC High Voltage Module

The High Voltage Module (HVM) located within the pressure vessel is a PCB tasked with converting input voltage of +12V from the Data Acquisition Module into a very high negative voltage to bias the conductive tissue equivalent plastic proportional counter. This conductive plastic proportional counter is biased to -1000V to create a uniform electric field within the TE sphere, in order to ionize particles that pass through the TEPC. The top and bottom of the HVM can be found in Figure 14.

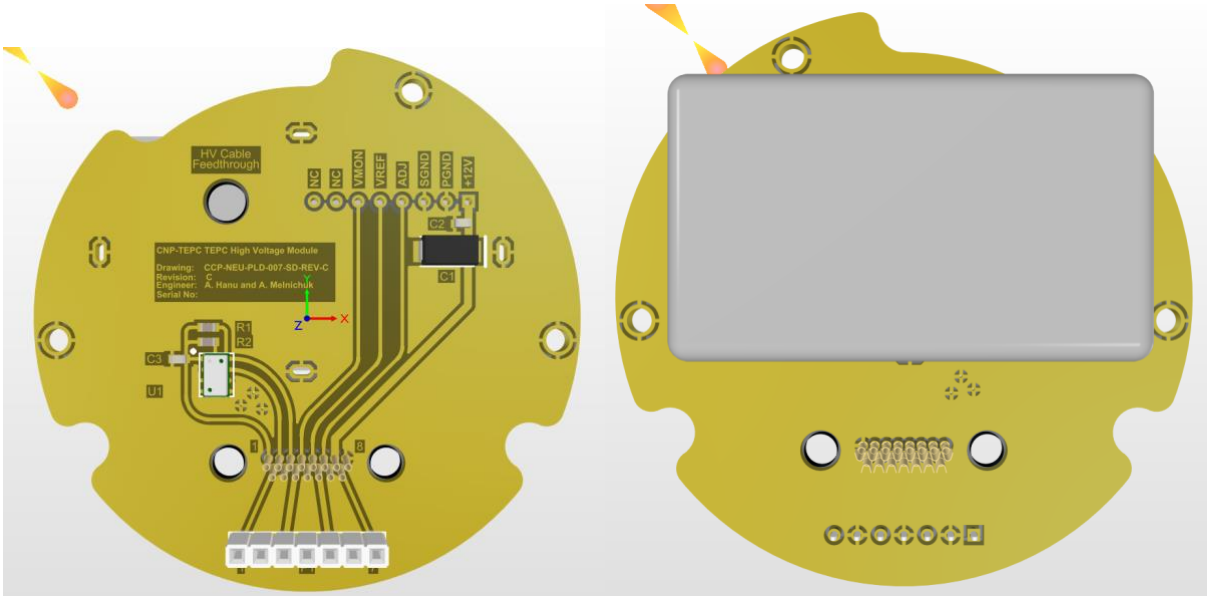

Figure 13: PCB view of the High Voltage Module.

The High Voltage Module is made up of a miniature high voltage biasing supply made by Advanced Energy. The miniature high voltage supply (P/N 1M12-N0.5-WS) is able to produce a voltage range from 0V to -1000V from an input voltage of 12V from the analog power converters on the Data Acquisition Module (DAM). The HV supply produces 0.5W of power, with a total current draw of 0.5 mA. The HV power supply has an adjustment voltage pin to control the output voltage leading to the conductive plastic rings, to produce the voltages within the operating range.

Output voltage from the HV power supply is determined by the input voltage adjustment compared with the reference voltage of +12V. This voltage adjustment value is determined by a circuit on the DAM via a digital to analog converter. This voltage adjustment value is set by the FPGA, which is transmitted to a DAC via SPI. The DAC translates this transmitted voltage into an analog voltage value comparable to the High Voltage power supply's reference voltage. The output voltage is then connected back to the high voltage power supply where it is compared with the reference voltage.

Power Startup Sequence

When power is applied to the payload subsystem, the High Voltage Module is not powered, preventing any risk of shock. The HVM on/off state is controlled by the +12V analog power supply. The analog power supply is controlled by the Spartan 6 onboard FPGA. By default, when the payload is supplied power, the +12V analog regulator is not powered. To enable this regulator, the FPGA must send a high signal, which will eventually turn on the HVM. Due to this configuration, there is no risk of the HVM having power supplied to it when the power cable is connected, therefore eliminating the risk of electric shock.

Fail Case Scenarios

The High Voltage Module is located under the TEPC Module and TEPC, within the detector vessel as well as the ACD. Physical access to the High Voltage Power Supply and High Voltage Module is not possible from any external section of the payload. A cross sectional view of the payload can be found in Figure 15 below with a label showing the High Voltage Power Supply.

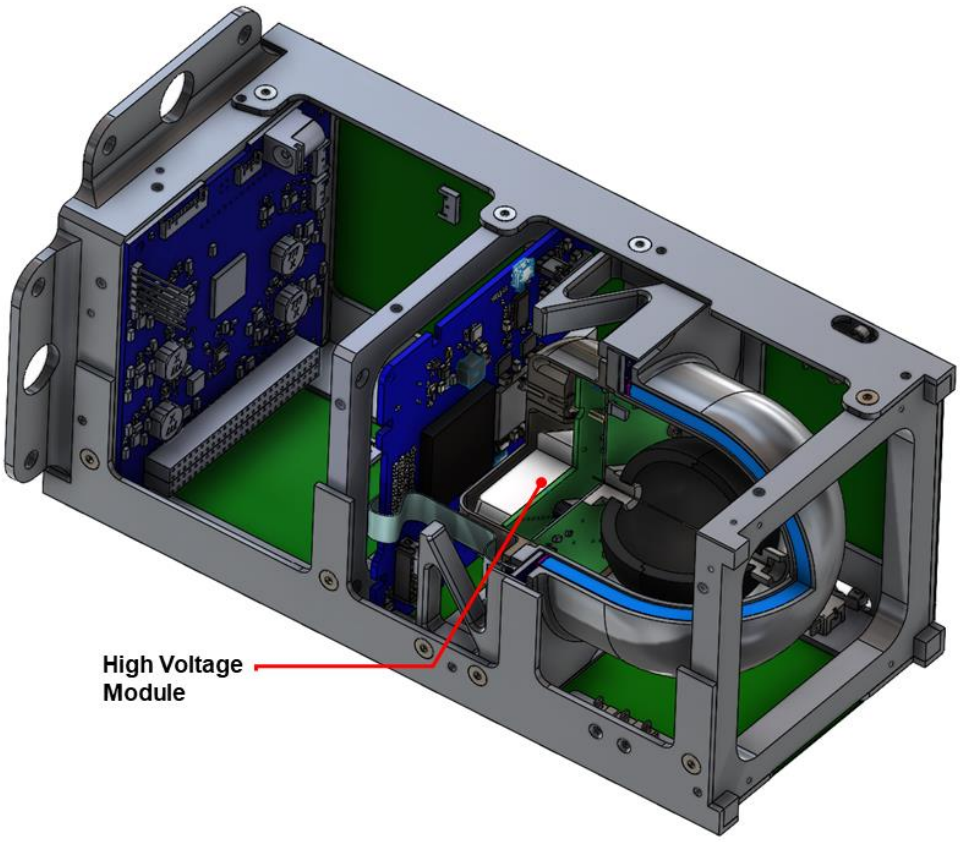

Figure 14: Cross section of the CNP-TEPC with a cutaway showing the nested location of the High Voltage Power Supply.

If failure is to occur, it could happen in these possible ways:

- The anode wire mount becomes disconnected and shorts out with the side of the TE sphere
- The TE sphere mount becomes disconnected and shorts out with the aluminum pressure vessel housing
- Hardware failures on the High Voltage Module

The payload has been grounded in such a way that if any of these fail case scenarios were to take place, the associated power would be properly grounded to the chassis. The payload is grounded with a star point grounding system, with the single grounding point in the Electrical Power System (EPS) in case of a short circuit or hardware failure. As the payload will not have access to a true ground, each of the chassis sections will have a resistor to prevent a current loop within the satellite's chassis. The Grounding Diagram, shown in Figure 16, shows this main path the current will take in each of the failure conditions.

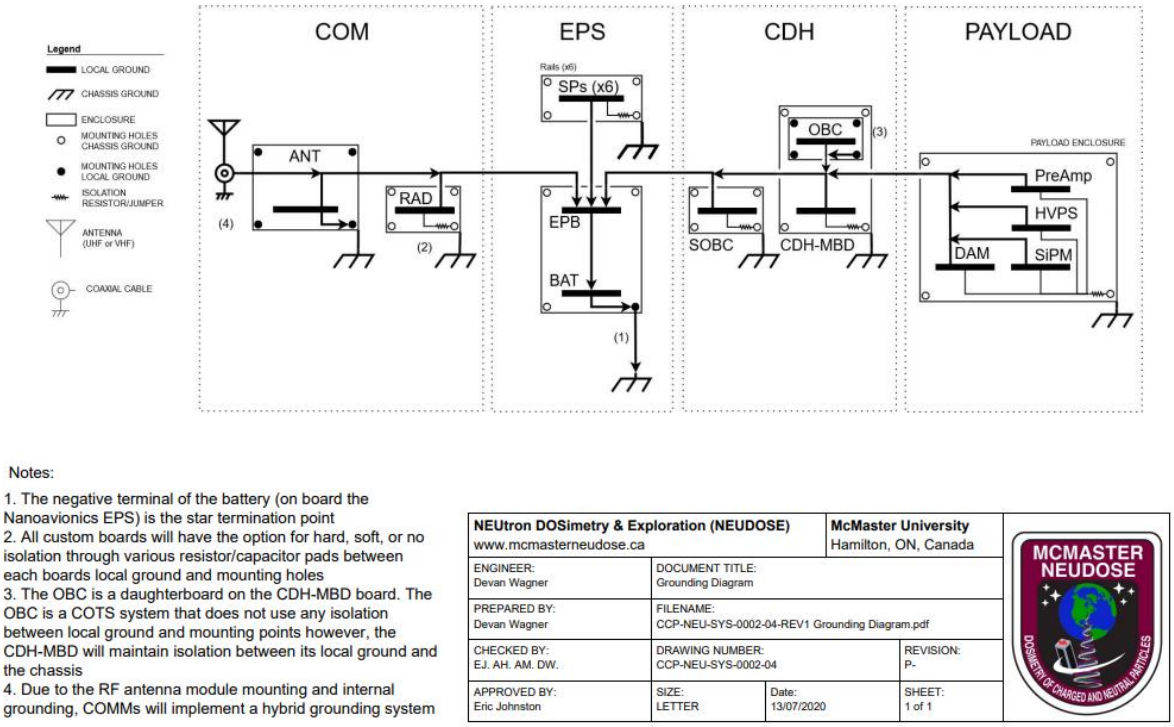

Notes:

1. The negative terminal of the battery (on board the Nanoavionics EPS) is the star termination point
2. All custom boards will have the option for hard, soft, or no isolation through various resistor/capacitor pads between each boards local ground and mounting holes
3. The OBC is a daughterboard on the CDH-MBD board. The OBC is a COTS system that does not use any isolation between local ground and mounting points however, the CDH-MBD will maintain isolation between its local ground and the chassis
4. Due to the RF antenna module mounting and internal grounding, COMMs will implement a hybrid grounding system

NEUtron DOSimetry & Exploration (NEUDOSE) www.mcmasterneudose.ca			**McMaster University** Hamilton, ON, Canada
ENGINEER: Devan Wagner	DOCUMENT TITLE: Grounding Diagram		
PREPARED BY: Devan Wagner	FILENAME: CCP-NEU-SYS-0002-04-REV1 Grounding Diagram.pdf		
CHECKED BY: EJ. AH. AM. DW.	DRAWING NUMBER: CCP-NEU-SYS-0002-04		REVISION: P-
APPROVED BY: Eric Johnston	SIZE: LETTER	Date: 13/07/2020	SHEET: 1 of 1

Figure 15: Grounding Diagram for the NEUDOSE CubeSat.

In the case of the anode wire becoming disconnected from the TEPC and coming into contact with the TE sphere, the excess current from the TEPC would pass through the anode wire into the TEPC Preamp board, into the main route to the Electrical Power Board, through the Battery, and eventually grounded to the chassis of the payload. Similarly, if the negatively biased TEPC were to become detached from the Preamp board and come into contact with the pressure vessel, the power would flow through the pressure vessel into the chassis.

For hardware failures, both the TEPC Preamp board and the High Voltage Module are mounted within the pressure vessel. In the scenario where there is a hardware failure, the excess current will flow through the boards into the pressure vessel, and ultimately into the CubeSat's chassis. In any case of failure, the current will flow through the main current path to the EPS or to the grounded chassis, due to the several grounded layers between the HVM and the external section of the CubeSat.

TEPC Front End Electronics

The TEPC Front End Electronics (FEE) are responsible for tracking timing events for particle interactions as well as amplifying the amount of charge absorbed from the anode wire during said interactions. The Front End Electronics are housed on the TEPC Readout Module, located within the pressure vessel.

When a particle interaction occurs within the TEPC, the ionized charge is absorbed by the anode wire, running through the centre of the TEPC. This charge flows through the anode wire to the

TEPC Module, where it is processed through several different filters and amplifiers. The signal is amplified in a three stage structure, with the ability to determine an adjustment voltage in the final stage. This adjustment voltage is transmitted to a DAC from the FPGA via SPI, corresponding to a voltage between 0 and 5V. The adjustment voltage can amplify the acquired signal further if a low amount of charge is deposited in the anode wire. After the final amplification stage, the signal passes through an analog to digital converter where the acquired charge is digitized and transmitted to the FPGA.

1.5.5 Silicon Photomultipliers (SiPM)

The Silicon Photomultipliers (SiPMs) are used to detect UV waves and release a photocurrent to be used to learn information about the radiation. The SiPMs are used in the Anti-Coincidence Detector to differentiate between charged and neutral particle interactions. The SiPMs detect UV rays produced by ionizing radiation interacting with the outer shell of the plastic scintillator. The SiPMs are mounted on the SiPM module, receiving power from the SiPM Bias Power Supply. The photocurrent is read out by the Citiroc ASIC located on the DAM, made specifically to digitize SiPM photocurrent values. The 32 SiPMs included on the SiPM Module are the SensL MicroFJ-30035-TSV SiPMs. TSV represents Through Silicon Via (TSV) technology, which allows the manufacturer to place the electrical contacts on the bottom side using a ball grid array (BGA) and achieve a higher packaging density. Because the gain of SiPMs depends significantly on temperature and bias voltage, 4 surface temperature sensors are located at each corner for the SiPM Module to permit the bias voltage to be adjusted according to the average temperature across the board, thus maintaining a constant SiPM gain.

SiPM Module

Silicon Photomultipliers (SiPM) are used to detect UV waves and release photocurrent that can be used to learn information about the radiation. In our system they detect the UV rays released by the outer shell of the plastic scintillator when it comes in contact with ionizing radiation. LEDs are used to calibrate the SiPM to make sure that they can detect the different pulses of radiation correctly, or checking for malfunctions. Since the photocurrent is dependent on temperature, temperature sensors are also used to calibrate the SIPM module. There are 4 of these temperature sensors, each located near the four corners of the PCB. The SIPMs themselves are located in a ring around the hole in the centre of the PCB.

The SiPM module is connected via a FFC cable (the DAM ribbon cable) to the DAM. The module interfaces directly with the CITIROC, which digitizes the photocurrent so that it can be analyzed by the FPGA. The data from the temperature sensors are sent directly to the housekeeping ADCs where they are digitized and sent to the FPGA via SPI. The temperature sensors are also critical in determining the SiPM bias voltage as explained in the next section.

SiPM Bias Power Supply

The SiPMs require a specific voltage supply range in order to produce a photocurrent when UV waves are detected. This voltage bias is temperature dependent, and can range between 24V to 31V. The SiPM bias power supply circuitry is located on the Data Acquisition Module, and

provides 24V to 31V at 5 mA from a MAX1932 Avalanche Photodiode Bias Supply. This bias power supply takes an input voltage of 3.3V from the digital power converter on the DAM. The output voltage is driven by the SPI data transmitted to the MAX1932 chip from the Spartan 6 FPGA.

The Spartan 6 FPGA receives SPI feedback from the housekeeping analog to digital converters onboard the DAM, reporting the temperature of the four temperature sensors located on the SiPM Module. This temperature value is used to determine the bias voltage used for the SiPMs, ranging from 24V corresponding to cold temperatures, to 31V corresponding to warm temperatures. The output voltage and current are monitored by housekeeping ADCs and are reported to the Spartan 6 FPGA to ensure no errors occur between the temperature and the bias voltage for the SiPMs.

1.6 Thermal Control Plan

The flight duration of up to 20 hours means the flight may extend into the night, meaning two steady-states conditions may be reached, with and without significant solar radiation. To gain an understanding of the temperature ranges the payload is expected to experience during this mission, two preliminary steady-state thermal simulations (a hot case and a cold case) were conducted with COMSOL software. The

A brief overview of the simulation conditions follows. It is assumed the payload will experience no convective heat transfer, as ambient pressures of 5-10mbar are expected. The payload was geometrically simplified and is composed of materials including anodized Aluminum 6061-T6 and 304L stainless steel for structural components, and FR-4 and Silicon for PCB and solar boards. It is assumed the initial temperature for both cases is 293.15K, and the ambient temperature of the atmosphere is 230.15K. The former did not prove critical to the final resulting temperatures, while the latter is approximate of the typical ambient outside temperature on a previous mission (Figure 4. HASP Call for Payloads 2021). The final temperature range of the cold case was especially sensitive to modifications in the ambient temperature. Both the hot and cold cases heat-emission from PCB components, however the hot case included solar board heat generation while the cold did not. Select outer boundaries for the hot case had a constant heat flux of 1361W/m^2 to represent solar radiation, while the cold case did not. Cross sections of these simulations can be seen below in Figure 17. The hot case spans a temperature range of 278K (~5oC) to 325K (~52oC), which fits well within the operational temperature range of -20oCto 85oC for the most intolerant components of the payload. The cold case spans a significantly narrower temperature range of 231.5K (~-41.5oC) to 236.5K (~-37oC). This range is far below that of the operational temperature minimum (-20oC) for the CNP-TEPC, TEPC (both not pictured due to geometrical simplifications), and the HVM. Additionally, the solar boards experience the lower end of this temperature range, placing them outside of their operational temperature minimum of -40oC. These numbers should not be concerning as the payload geometry excluded any thermal solutions such as insulation and specialized coatings. Further transient simulation work will be performed in ANSYS to determine the extent to which these are required.

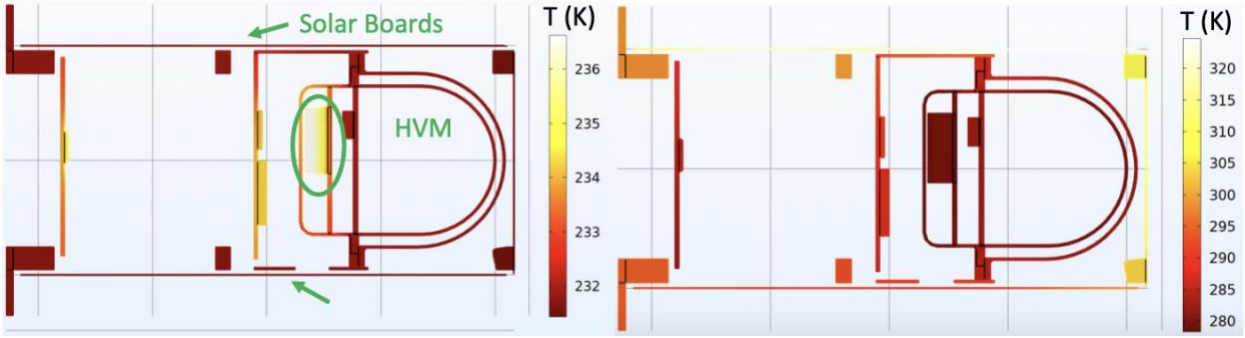

Figure 16: Cold (left) and hot (right) cases for the Payload.

2. Team Structure and Management

2.1 Team Organization and Roles

Amy Ling will act as the student team leader, where her management duties include submission of monthly status reports, attending and documenting teleconference calls, documentation, and liaising between the student group and the 3 faculty and industry advisors. Ms. Ling will also lead the development, integration, and testing of the CNP-TEPC instrument.

Leading the mechanical structure team is Gabriel Teichman. His duties include the design, construction, and integration of the payload structure. Mr. Teichman will ensure the appropriate interfacing of all components of the payload.

Connor Chandran leads the power team. His duties include the design, construction, and testing of the PDM to ensure that the electrical demands of every component of the payload will be handled accordingly.

Travis Ratnaharan leads the firmware team. His duties include the design, testing, and integration of payload firmware, including the packet structure and development of register files.

The project will receive guidance and funding from 3 faculty and industry advisors who will also be in communication with the group on a weekly basis. The 3 advisors are:

- Dr. Andrei R. Hanu, a senior scientist at the Bruce Power Nuclear Generating Station and an adjunct assistant professor in the Department of Physics & Astronomy at McMaster University. Dr. Hanu developed the CNP-TEPC instrument and NEUDOSE mission concepts and will provide guidance pertaining to the development of the mission and the science instrument.
- Dr. Soo-Hyun Byun, a professor in the Department of Physics & Astronomy at McMaster University. Dr. Byun will provide technical and theoretical guidance pertaining to the science instrument development.
- Dr. Eric Johnston, the chief innovation officer at the Nuclear Innovation Institute, a former HASP program student, and a co-principal investigator on the McMaster NEUDOSE mission.

The CNP-TEPC team is composed of 19 students and 3 faculty advisors. The structure of the team is summarized in Table 1.

Table 1: HASP team members, roles, and student statuses.

NAME	ROLE	STUDENT STATUS	CONTACT
AMY LING	Student Project Lead	Chemical & Biomedical Engineering IV	linga9@mcmaster.ca
GABRIEL TEICHMAN	Mechanical Lead	Mechanical Engineering & Management Alumni	teichmgd@mcmaster.ca

CONNOR CHANDRAN	Power Lead	Electrical Engineering & Management IV	chandrac@mcmaster.ca
TRAVIS RATNAHARAN	Firmware Lead	Engineering Physics IV	ratnahat@mcmaster.ca
XINGZHI CHEN	Instrument Scientist	Medical Physics, MSc	chengx4@mcmaster.ca
ROY SUN	Instrument Scientist	Medical Physics, MSc	sunr9@mcmaster.ca
NICK PHAN	Mechanical Team	Mechanical Engineering III	phann6@mcmaster.ca
JULIANA ONESI	Mechanical Team	Mechanical & Biomedical Engineering IV	onesij@mcmaster.ca
ALESSIA DI NARDO	Mechanical Team	Mechanical & Biomedical Engineering IV	dinardoa@mcmaster.ca
ARIELLE AINABE	Power Team	Engineering Physics II	ainabea@mcmaster.ca
BOBBY TANG	Firmware Team	Medical & Biological Physics IV	tangb12@mcmaster.ca
GRAHAM POWER	Firmware Team	Mechatronics Engineering III	powerg@mcmaster.ca
JORDAN BIERBRIER	Firmware Team	Mechatronics Engineering & Management III	bierbrj@mcmaster.ca
RICARDO POLO	Firmware Team	Physics IV	polor@mcmaster.ca
LIAM TAYLOR	Firmware Team	Computer Engineering VI	taylorl@mcmaster.ca
AYESHA SIDDIQI	Firmware Team	Electrical Engineering & Management V	siddiqia@mcmaster.ca
ADAM TYEDMERS	Thermal Team	Materials Science & Engineering IV	tyedmera@mcmaster.ca
MICHAEL CHEN	Electrical & Power Systems	Engineering Physics IV	cheny263@mcmaster.ca
NICHOLAS VRZOVSKI	Mission Operations & Controls	Engineering Physics III	vrzovskn@mcmaster.ca

The student group regularly meets on a weekly basis and also confers with at least one advisor once a week. In addition, the team maintains active communication and consistent documentation through web interfaces such as Slack and Confluence.

It is anticipated that all 19 members and 2 advisors will attend integration and testing at the CSBF in 2021. The same 21 individuals are expected to participate in flight operations at Ft. Sumner in 2021.

2.2 Timeline and Milestones

The CNP-TEPC team has identified four stages to complete before HASP 2021: design, fabrication, integration & testing, and flight of the mission. Each phase and its expected duration, as well as key milestones, are outlined in table 2. A full Gantt chart of the mission schedule can be found in Appendix A.

Table 2: The phases of the CNP-TEPC project, key milestones, and anticipated durations.

Phase/Milestone	**Date(s)**	**Description**
Phase A: Design	Oct. 2020 – Mar. 2021	Design of all physical components, Development of all electronic systems for the TEPC, ACD, DAM, and PDM.
Mechanical Design Review	Dec. 2020	Finalization of mechanical design.
Electronics Design Review	Mar. 2021	Finalization of electronics design.
Phase B: Fabrication	Jan. – Apr. 2021	Ordering, fabrication & inspection of all components.
Preliminary PSIP Document Due	Apr. 2021	Preliminary document of specification & integration plan.
Phase C: Integration & Testing	Feb. – Aug. 2021	Integration of components into housing, thermal vacuum, vibration/shock & radiation testing. Instrument calibration. Integration at CSBF.
Final PSIP Document Due	Jun. 2021	Final document of specification & integration plan.
Final FLOP Document Due	Jul. 2021	Final document of flight operations plan
Phase D: Flight & End of Mission	Sep. – Nov. 2021	Flight preparation operations. Recover, packing & return. End of mission documentation.

2.3 Anticipated Participation in Integration and Launch operations

The CNP-TEPC has been designed for autonomous operation and minimal operations during integration and throughout flight is expected. During integration, we require the payload to be bolted to the mounting plate and the serial and power connectors to be attached. All other assembly of the payload will be done prior to integration with the HASP balloon. We anticipate the following steps for successful payload integration:

1. Provide the latest payload mechanical and electrical interface control documents.
2. Pre-integration inspection to confirm HASP compliance (mass, voltage, and current).
3. Test instrument power up using HASP bench test hardware.
4. Test instrument telemetry using HASP bench test hardware.
5. Mount instrument to HASP platform.
6. Test instrument power up using actual HASP flight hardware.
7. Test instrument telemetry using actual HASP flight hardware.
8. Perform pre-flight thermal vacuum testing.
9. Test instrument communications throughout flight. Verify with the HASP interface.

During flight, the CNP-TEPC will operate autonomously and send a full dataset using the serial downlink every 10 minutes.

3. Payload Interface Specifications

3.1 Weight Budget

The total weight budget for the payload is outlined in Table 3 below. The total weight of the payload was calculated to be 1865g. A 10% margin of error was incorporated for each component. The total allowable weight for a small payload is 3000g resulting in a worst-case margin of 1055g below the allowable weight limit.

Table 3: Weight budget for the HASP 2021 CNP-TEPC.

Description	Part Number	Mass (g)	Uncertainty	Method Of Measurement
Anti-Coincidence Detector (ACD) Components				
SiPM Module	CCP-NEU-PLD-004-02-PC-REV-A	19	1.9	Measured mass of current manufactured board variant
ACD Scintillator	CCP-NEU-PLD-008-PF	68	6.8	Based on CAD estimate
ACD Lid	CCP-NEU-PLD-012-PF	90	0.9	Based on CAD estimate
Optical Coupling Gasket	CCP-NEU-PLD-010-PF	4	0.04	Based on CAD estimate
CNP-TEPC Assembly				
Data Acquisition	CCP-NEU-PLD-005-PC-	68	2	Measured mass of current

Module	REV-B			manufactured board variant
Payload Housing	CCP-NEU-PLD-001-PF	121	1.21	Measured mass of first article machined component
M2x0.4x6mm - DAM Screws (Qty. 4)	ISO 4762	1.2	0.012	Based on CAD estimate
M2.5x0.45x6.5mm - ACD Lid Screws (Qty. 4)	ISO 10642	1.2	0.012	Based on CAD estimate
M3x0.5x8mm - TEPC Screws (Qty. 4)	ISO 10642	2	0.02	Based on CAD estimate
Detector Vessel Assembly				
Detector Vessel Lid	CCP-NEU-PLD-0013-PF	95	0.95	Based on CAD estimate
Detector Vessel Base	CCP-NEU-PLD-003-SA	179	1.79	Measured mass of first article machined component
Indium O-Ring	CCP-NEU-PLD-0011-PF		0	Based on CAD estimate
M3x0.5x6mm (QTY 12) Detector Vessel Screws	ISO 4762	9.6	0.096	Based on CAD estimate
Tissue Equivalent Proportional Counter (TEPC)	CCP-NEU-PLD-002-SA	45	4.5	Based on CAD estimate
Preamplifier Module	CCP-NEU-PLD-006-PC	10	1	Measured mass of current manufactured board variant
High Voltage Module	CCP-NEU-PLD-007-PC-REV-C1	20	2	Measured mass of current manufactured board variant
Mechanical Subsystem				
Rails	CCP-NEU-MEC-001-01	209	20.9	Based on CAD estimate
(+) Z Plate	CCP-NEU-MEC-001-02	86	8.6	Based on CAD estimate
(-) Z Plate	CCP-HSP21-001-PF	167	16.7	Based on CAD estimate
Support Tray	CCP-NEU-MEC-001-04	60	6	Based on CAD estimate
M3x0.5x8mm (QTY 36) - Rail Mounting	ISO 10642	18	1.8	Based on CAD estimate
M2x0.4x6mm - Solar Panel Screws (Qty. 28)	ISO 4762	8.4	0.84	Based on CAD estimate
M2x0.4x6mm - PDM Screws (Qty. 4)	ISO 4762	1.2	0.12	Based on CAD estimate
Electrical Power Subsystem				
Solar Panel (+Y)	CCP-NEU-EPS-002-1-PC-REV-P	92	9.2	Based on CAD estimate

Solar Panel (-Y)	CCP-NEU-EPS-002-1-PC-REV-P	92	9.2	Based on CAD estimate
Solar Panel (+X)	CCP-NEU-EPS-002-1-PC-REV-P	92	9.2	Based on CAD estimate
Solar Panel (-X)	CCP-NEU-EPS-002-1-PC-REV-P	92	9.2	Based on CAD estimate
Solar Panel (+Z)	CCP-NEU-EPS-002-2-PC-REV-P	46	4.6	Based on CAD estimate
Inhibit Switch 1	ZM10E10F01	2	0.2	Based on Manufacturer Spec Sheet
Inhibit Switch 2	ZM10E10F01	2	0.2	Based on Manufacturer Spec Sheet
Inhibit Switch 3	ZM10E10F01	2	0.2	Based on Manufacturer Spec Sheet
Inhibit Switch 4	ZM10E10F01	2	0.2	Based on Manufacturer Spec Sheet
Power Distribution Module	CCP-HSP21-001-PC	100	10	Based on CAD estimate
Cabling	Misc	60	20	Best Estimate
	Total	**1864.6**	**80.23**	
	Margin	**1055.17**		

3.2 Power Budget

For the HASP 2021 mission, we are sending the CNP-TEPC assembly, the Electrical Power System solar panels as well as the Power Distribution Module. Overall, this creates a peak power draw of around 3.8W, well below the 15W allotted to small payloads. The 3.8W power draw is made up primarily from the power requirements from the CNP-TEPC instruments and DAM. Table 4 shows the expected power draw for the electronic components in the payload.

Table 4: Power Consumption values for the HASP 2021 CNP-TEPC.

Payload	**PAY**	**Peak Current (mA)**	**Power Consumption (mW)**		**Power Source**	**Voltage (V)**
			Stand By	**Operation**		
Tissue Equivalent Proportional Counter	TEPC	N/A	N/A	N/A	N/A	N/A
--> Preamplifier Module	PAM	1.2	5	14	DAM	+5 / -5
--> High Voltage Module	HVM	200	5	2400	DAM	+12
Data Acquisition Module	DAM	103	1000	1235	PDM	+12

Electrical Power Subsystem	EPS	Peak Current (mA)	Power Consumption (mW)		Power Source	Voltage (V)
			Stand By	Operation		
Power Distribution Module	PDM	44	80.8	143.12	HASP	+30V

The current draw in the High Voltage Module is for when the High Voltage Power Supply is active. To create a bias voltage of -1000 V the high voltage power supply has a current draw of 200mA at 12V, using 2.4W alone. For the majority of the mission the High Voltage Module will not be active, drawing much less power than the 2.4W allotted to it. A detailed outline of the power draws can be found in Figure 12 above in section 1.5.1. The power usage in this block diagram is based off of a worst-case scenario with all components using power enabled.

3.3 Downlink Serial Data

The CNP-TEPC payload produces two spectra of data stored as 2-byte values in 16,384 bins, which will make up most of the data produced. Including 12 start and stop bytes, each data set will include 86 bytes of "housekeeping" data, 2 GPS measurements at 125 bytes each, and 2 bytes of XOR Redundancy Check information, making each transmitted file 65.916 kB in size. Spectra will be collected once every 10 minutes, requiring 110 bytes/s to be transferred. Using the 8-N-1 encoding scheme, the required downlink will be 110 bytes/s · 9/8 · 8 bits/1 byte = 990 bits/s - this falls below the upper limit of 1200 bps. The data is going to be stored locally on the payload, to test the data storage and recovery capabilities of the CNP-TEPC.

Data packet table is available in Appendix C.

3.4 Uplink Serial Commanding

We intend to use the serial uplink, but all commands will be kept under the two byte limit. Serial commands to toggle the radio on and off will be utilized.

3.5 Analog Downlink

We will not be using analog downlink.

3.6 Discrete Commanding

We will not be using discrete commanding.

3.7 Payload Location and Orientation Request

We do not have a preference for the location of the CNP-TEPC. We only request that the z-axis of the CNP-TEPC aligns with the gondola.

3.8 Special Requests

The CNP-TEPC uses two items on the Hazardous Materials List that are crucial to its operation: a high voltage module and a pressure vessel. Both of these items have been flown on previous HASP missions in 2017 and 2018. Additionally, extensive analysis has demonstrated that these components should not cause issues during flight.

The High Voltage Module is mounted into the base of the pressure vessel and supplies a potential of 800-1000V to bias the anode wire in the TE sphere, also located within the pressure vessel. This is critical to the operation of the CNP-TEPC to detect ionizing particle radiation. When particles interact with the TE sphere, the current travels through the anode wire which is soldered to the preamplification module. All parameters assigned to the TEPC allow for a resulting lineal energy spectrum of human adipose tissue. Due to the startup sequence configuration and the grounding of the HVM, we do not expect any safety concerns when handling the CNP-TEPC. This is explained in more detail in Section 1.5.4.

The Detector Vessel houses the TEPC detector and is backfilled with 20-40 torr of tissue-equivalent propane. It is crucial to isolate the interior of the detector vessel from the atmosphere to maintain the composition of the tissue-equivalent gas. This mixture of propane, carbon dioxide and nitrogen allow for the data collected to be comparable to human adipose tissue. As the detector vessel has flown on HASP 2017 and 2018, and with minimal changes to the design, we do not expect any safety concerns associated with this component. As further proof that the component poses no concern, a transient structural simulation has been completed using Ansys 2019. This simulation is shown in Appendix D. Multiple scenarios were modelled to simulate the vacuum in the pressure vessel, backfilling with TE gas, and the low-pressure interior in a space vacuum environment. Additionally, a time-stepped depressurization is included to address a Nanoracks requirement. The Nanoracks pressure limits defined by NRCSD IDD 4.3.8 state that the payload must be capable of meeting at minimum a 0-104.8 kPa pressure range with a minimum depressurization rate of 1 kPa/s. The static simulations indicate a factor of safety of 3.8 with a conservative model and the buckling analysis load factors are all above 70, so there should be no issues with buckling under the specified loading scenarios.

Both the high voltage module and pressure vessel have completed two successful HASP missions and have been extensively bench tested so neither component should be considered a safety concern during HASP 2021.

4. Preliminary Drawings and Diagrams

The following documents are attached for the CNP-TEPC:

- CNP-TEPC Payload Assembly
- HASP 2021 Payload Assembly
- HASP 2021 Payload Full Assembly
- HASP Mounting Plate

Further drawings are available upon request.

REVISIONS				
ZONE	REV.	DESCRIPTION	DATE	APPROVED
	P-	INITIAL RELEASE	2020-08-14	

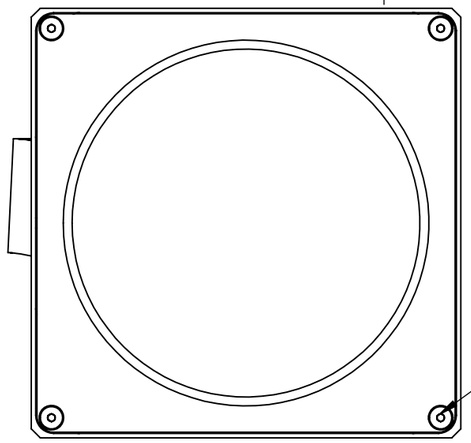

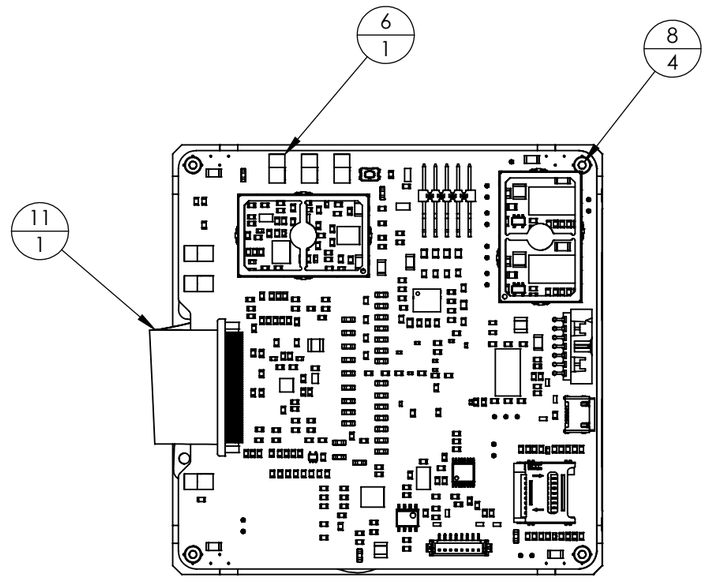

VIEW B

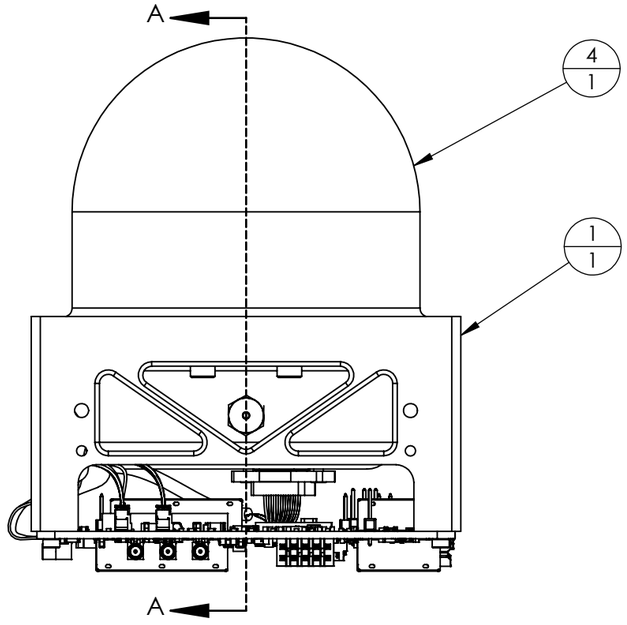

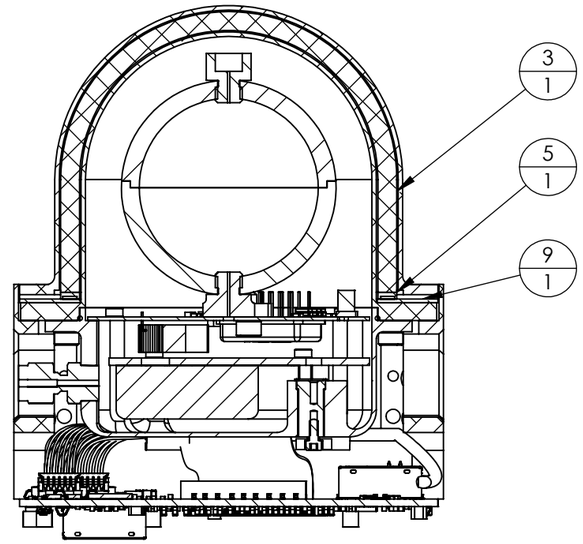

SECTION A-A

ITEM NO.	PART NUMBER	DESCRIPTION	QTY.
1	CCP-NEU-PLD-001-PF	CNP-TEPC HOUSING	1
2	CCP-NEU-PLD-001-SA	CNP-TEPC PRESSURE VESSEL	1
3	CCP-NEU-PLD-008-PF	ACD SCINTILLATOR	1
4	CCP-NEU-PLD-009-PF	ACD LID	1
5	CCP-NEU-PLD-010-PF	OPTICAL COUPLING GASKET	1
6	CCP-NEU-PLD-008-PC-FLIGHT	DATA ACQUISITION MODULE	1
7	91263A824		4
8	91292A831		4
9	SiPM Mockup		1
10	CCP-NEU-PLD-001-WD	PV-DAM WIRE HARNESS ASSEMBLY	1
11	CCP-NEU-PLD-002-WD	SiPM RIBBON CABLE	1
12	91263A423		4
13			2

△3 PRIME FASTENER THREADS WITH LOCTITE 7649 BEFORE APPLYING LOCTITE 242 (BLUE) TO INDICATED FASTENERS.

△2 FASTENERS TO BE TIGHTENED USING TORQUE WRENCH AS PER NEUDOSE MECHANICAL FASTENING DOCUMENT CCP-NEU-XXX.

1. REFER TO NEUDOSE DOCUMENT CCP-NEU-PLD-001 FOR ASSEMBLY INSTRUCTIONS AND PREPARATION STEPS TO SEAL AND FILL PRESSURE VESSEL.

NOTES: UNLESS OTHERWISE SPECIFIED

METRIC

THIRD ANGLE PROJECTION

DRILL HOLE SIZE	TOLERANCE
0.35 THRU 3.20	+0.10 / -0.03
3.21 THRU 6.40	+0.13 / -0.03
6.41 THRU 12.70	+0.15 / -0.05
12.71 THRU 19.00	+0.20 / -0.05
19.01 THRU 25.40	+0.25 / -0.08

UNLESS OTHERWISE SPECIFIED:
DIMENSIONS ARE IN MILLIMETERS.
TOLERANCES ARE:
X.X ±0.25 ANGLES: ± 0°- 30'
X.XX ±0.13 CHAMFERS: ±5°

MATERIAL

FINISH

DATE 2020-08-01
DRAWN N. PHAN
CHECKED
DESIGN G. TEICHMAN
APPROVED

NEUtron DOSimetry & Exploration CubeSat Project
McMaster University

TITLE: CNP-TEPC PAYLOAD ASSEMBLY

SIZE B | DWG. NO. CCP-NEU-PLD-001-AD | REV P-

SCALE 3:4 | DO NOT SCALE DRAWING | SHEET 1 OF 2

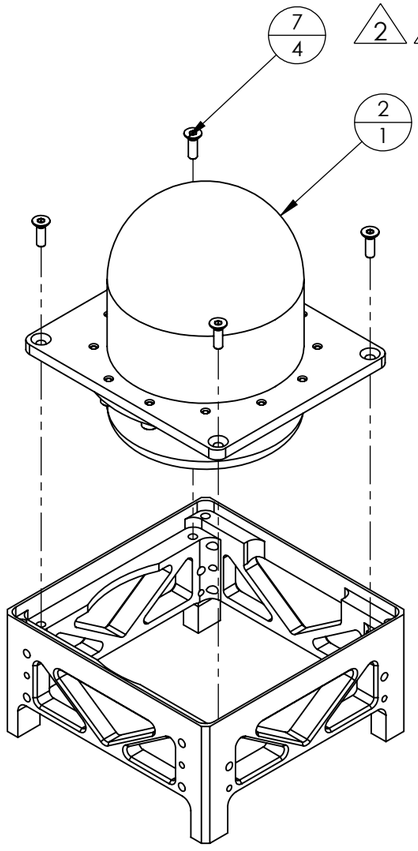

PRESSURE VESSEL INSTALLATION

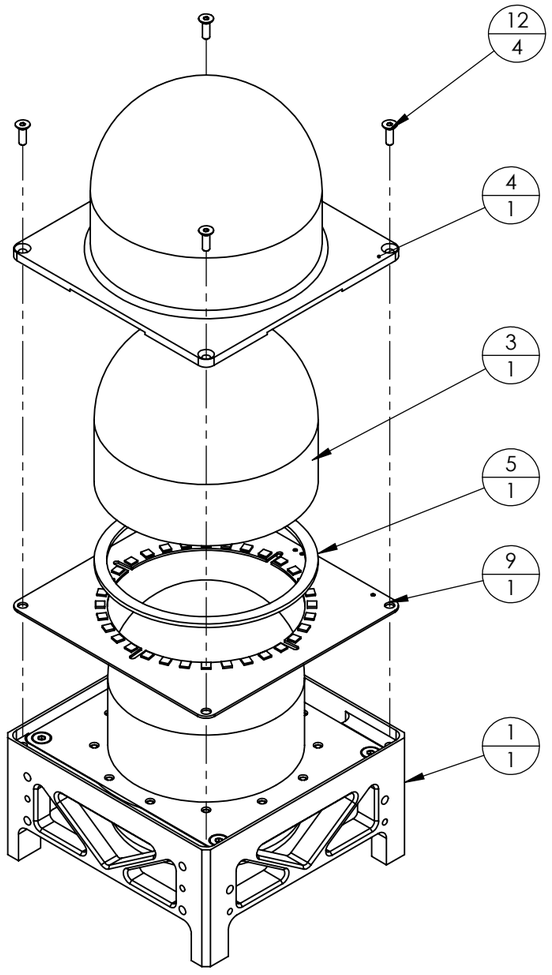

ACD INSTALLATION

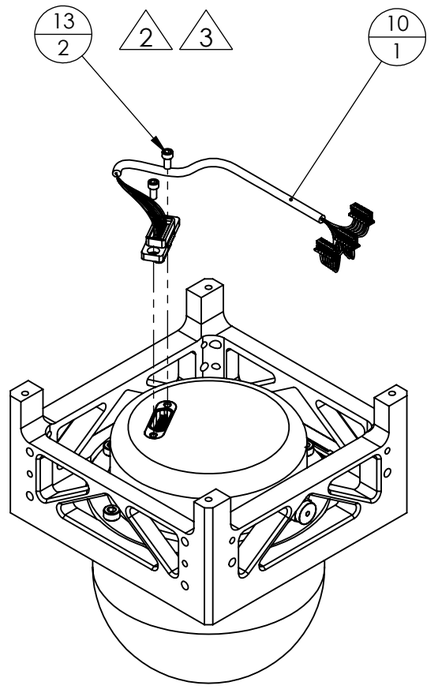

DAM-PV WHA INSTALLATION

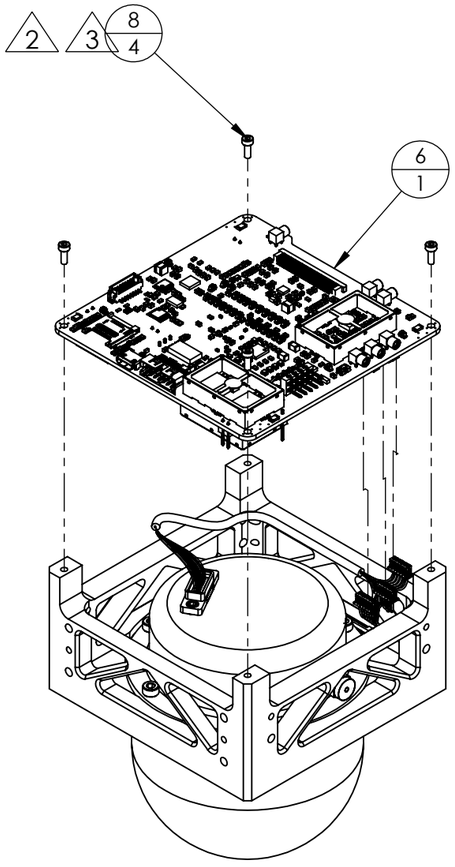

DAM INSTALLATION

NEUtron DOSimetry & Exploration CubeSat Project McMaster University		
TITLE: CNP-TEPC PAYLOAD ASSEMBLY		
SIZE B	DWG. NO. CCP-NEU-PLD-001-AD	REV -
SCALE 1:2	DO NOT SCALE DRAWING	SHEET 2 OF 2

REVISIONS				
ZONE	REV.	DESCRIPTION	DATE	APPROVED

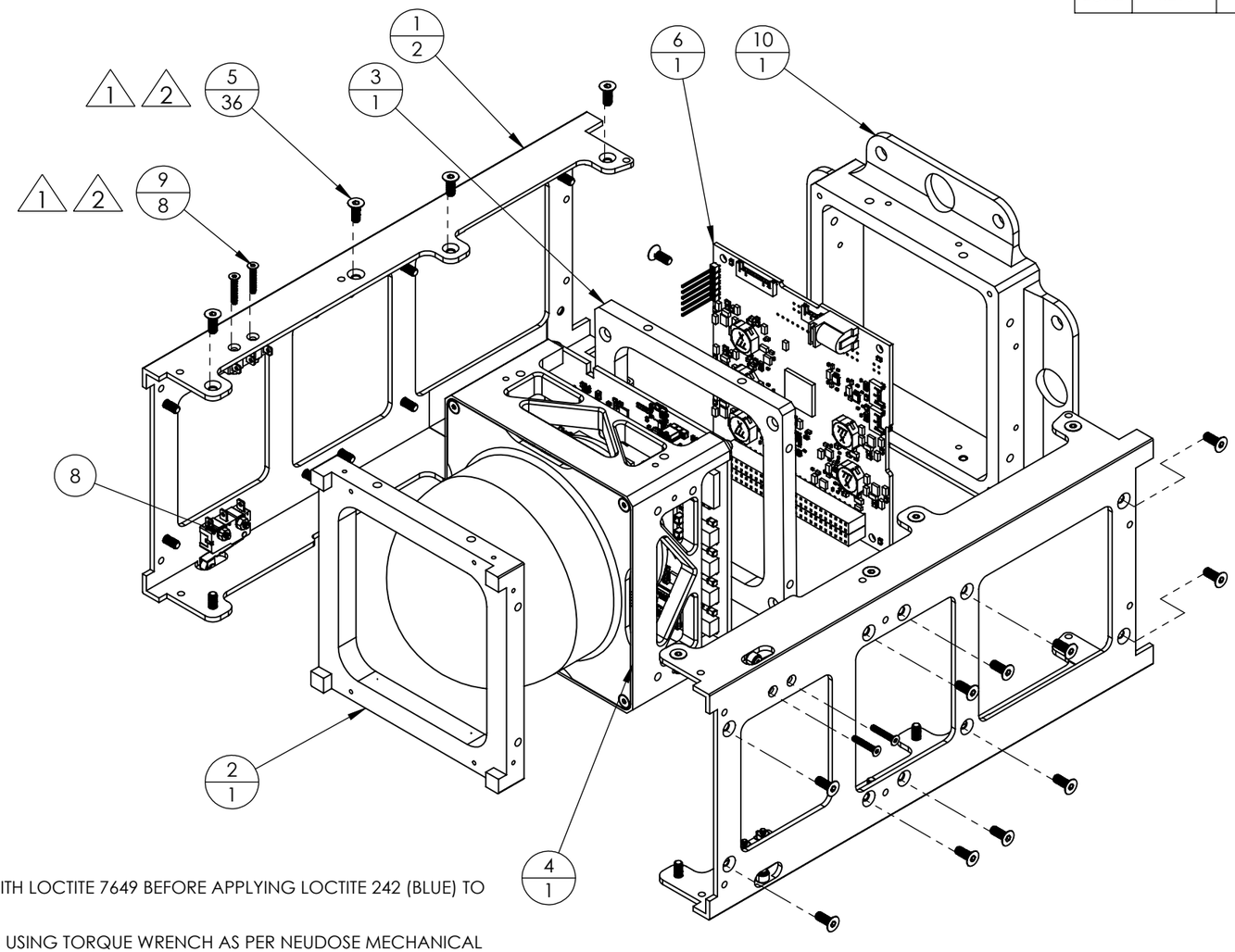

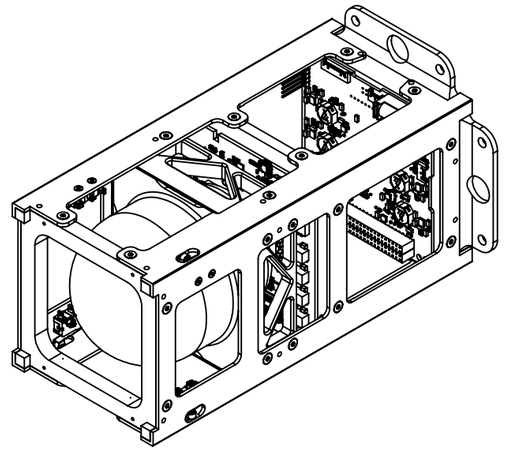

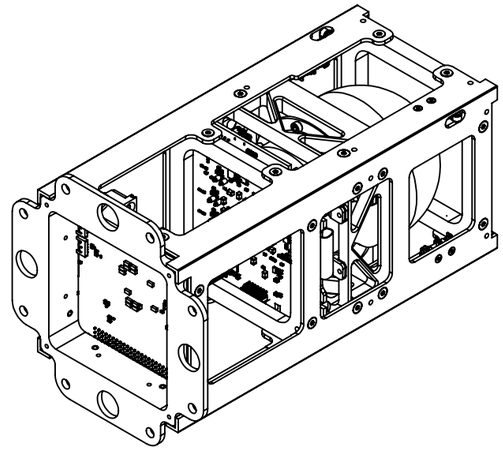

2 PRIME FASTENER THREADS WITH LOCTITE 7649 BEFORE APPLYING LOCTITE 242 (BLUE) TO INDICATED FASTENERS.

1 FASTENERS TO BE TIGHTENED USING TORQUE WRENCH AS PER NEUDOSE MECHANICAL FASTENING DOCUMENT CCP-NEU-XXX.

NOTES: UNLESS OTHERWISE SPECIFIED

ITEM NO.	PART NUMBER	DESCRIPTION	QTY.
1	RLS_R4_Frozen	STRUCTURE RAILS	2
2	ZTP_R4_Frozen	Z+ TRAY	1
3	TRY_R4_Frozen	MID Z TRAY	1
4	CCP-NEU-PLD-001-AD	PAYLOAD ASSEMBLY	1
5	91294A128	BLACK ALLOY STEEL FLAT-HEAD SOCKET CAP SCREW	36
6	SBX PDM	POWER DISTRIBUTION MODULE	1
7	zm10e10f01	INHIBIT SWITCH	4
8	90725A010	M2x0.4 NUT	8
9	93395A147	M3x0.5 BLACK ALLOY STEEL FLAT-HEAD SOCKET CAP SCREW	8
10	CCP-HSP21-001-PF		1

METRIC

THIRD ANGLE PROJECTION

DRILL HOLE SIZE	TOLERANCE
0.35 THRU 3.20	+0.10 / -0.03
3.21 THRU 6.40	+0.13 / -0.03
6.41 THRU 12.70	+0.15 / -0.05
12.71 THRU 19.00	+0.20 / -0.05
19.01 THRU 25.40	+0.25 / -0.08

UNLESS OTHERWISE SPECIFIED: DIMENSIONS ARE IN MILLIMETERS. TOLERANCES ARE:
X.X ±0.25 ANGLES: ± 0°- 30'
X.XX ±0.13 CHAMFERS: ±5°

MATERIAL

FINISH

DATE 2021-01-03
DRAWN N. PHAN
CHECKED
DESIGN
APPROVED 2021-01-08

NEUtron DOSimetry & Exploration CubeSat Project
McMaster University

TITLE: HASP 2021 PAYLOAD

SIZE **B** | DWG. NO. CCP-HSP21-002-AD | REV -

SCALE 1:2 | DO NOT SCALE DRAWING | SHEET 1 OF 2

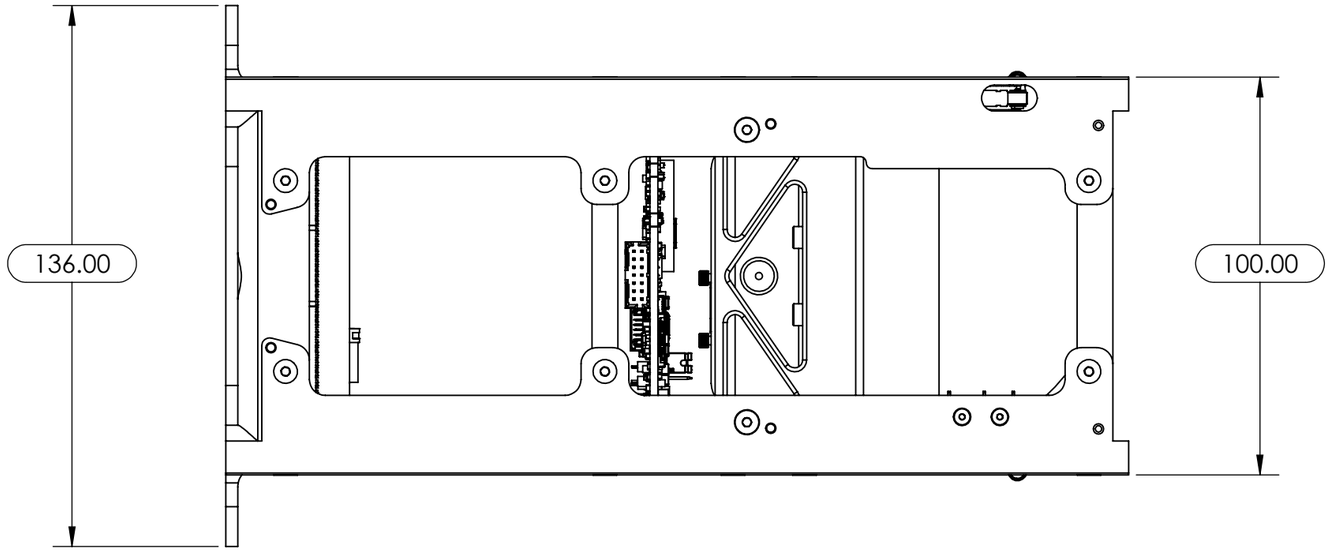

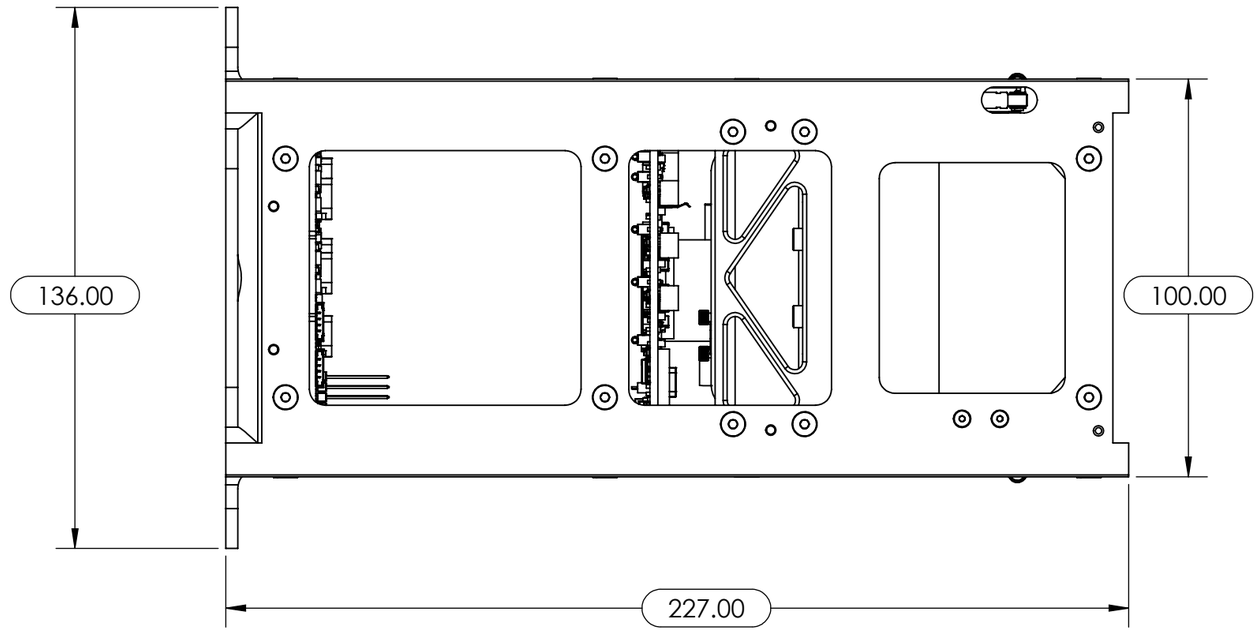

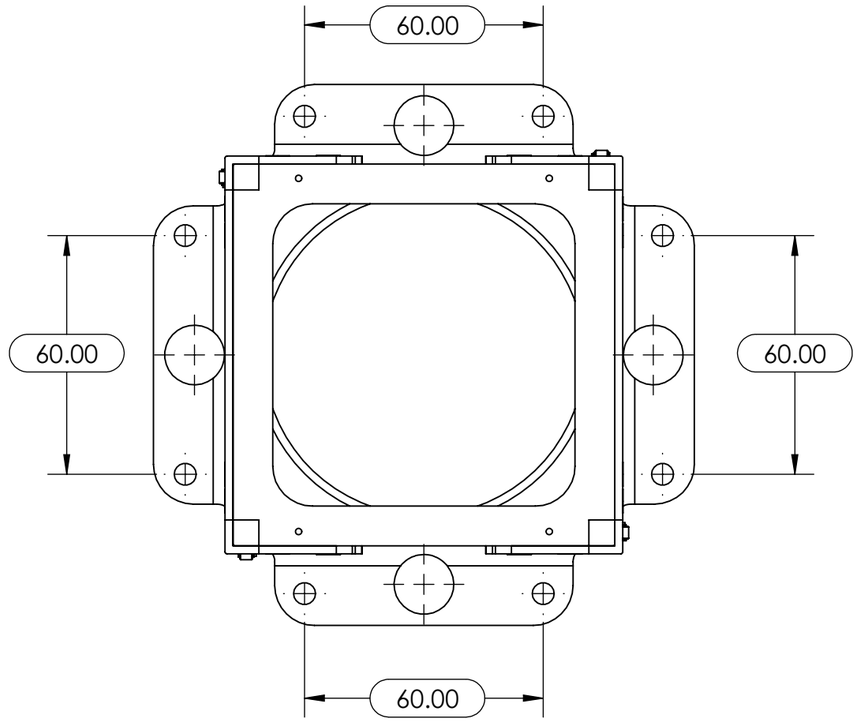

NEUtron DOSimetry & Exploration CubeSat Project McMaster University		
TITLE: HASP 2021 PAYLOAD		
SIZE B	DWG. NO. CCP-HSP21-002-AD	REV -
SCALE 2:3	DO NOT SCALE DRAWING	SHEET 2 OF 2

REVISIONS				
ZONE	REV.	DESCRIPTION	DATE	APPROVED

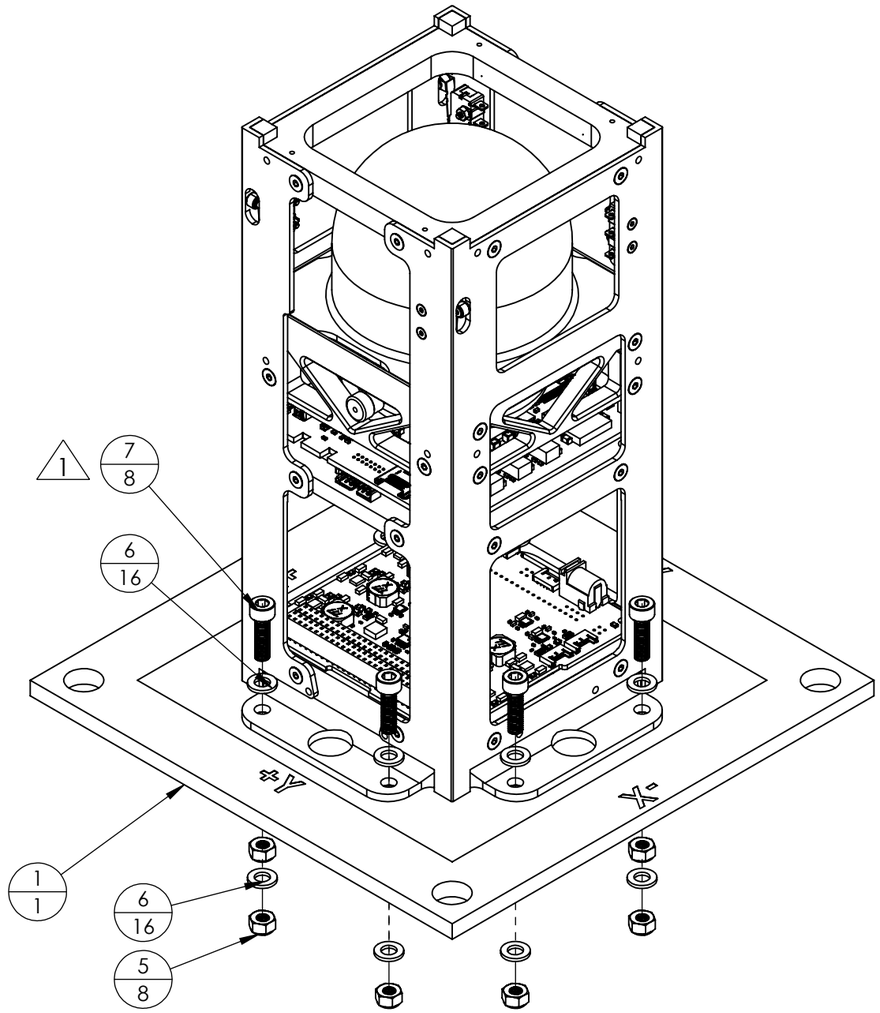

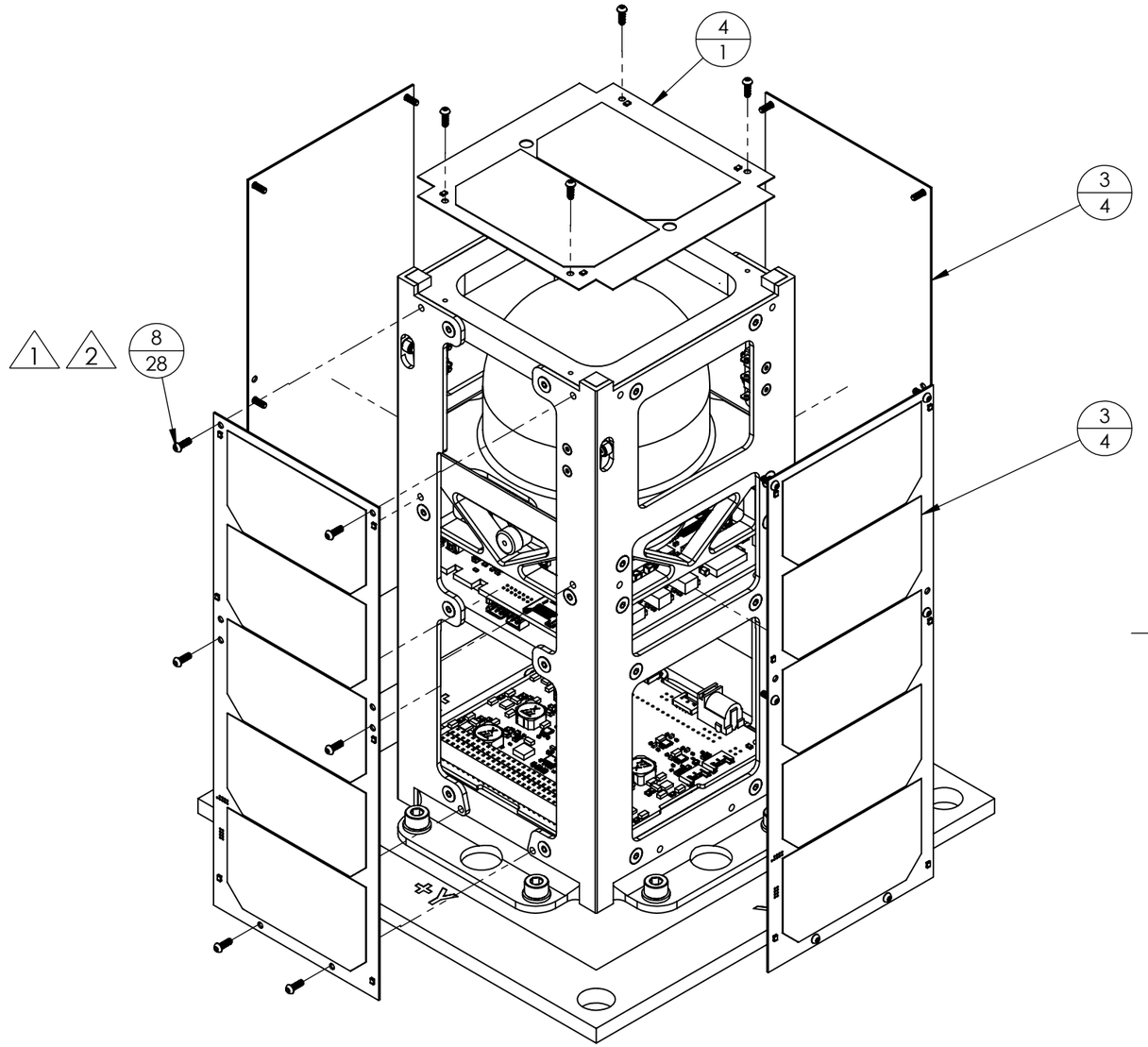

ITEM NO.	PART NUMBER	DESCRIPTION	QTY.
1	HASP MOUNT PLATE	MODIFIED HASP MOUNING PLATE	1
2	CCP-HSP21-002-AD	HASP 2021 PAYLOAD	1
3	CCP-NEU-EPS-002-1-PC-REV-P5- Long Solar Panel (-X)	LONG X/Y SOLAR PANEL	4
4	CCP-NEU-EPS-002-2-PC-REV-P5- Short Solar Panel	Z+ SOLAR PANEL	1
5	94645A102	CLASS 10, ZINC PLATED, M5 X 0.8 mm THREAD, 5 mm HIGH	8
6	98687A110	GENERAL PURPOSE STEEL WASHER FOR M5 SCREW SIZE, 5.500 mm ID, 10 mm OD	16
7	91290A238	BLACK-OXIDE ALLOY STEEL SOCKET HEAD SCREW M5 X 0.8 mm THREAD, 18 mm LONG	8
8	92095A453	BUTTON HEAD HEX DRIVE SCREW PASSIVATED 18-8 STAINLESS STEEL, M2 X 0.40 mm THREAD, 6mm LONG	28

2 PRIME FASTENER THREADS WITH LOCTITE 7649 BEFORE APPLYING LOCTITE 242 (BLUE) TO INDICATED FASTENERS.

1 FASTENERS TO BE TIGHTENED USING TORQUE WRENCH AS PER NEUDOSE MECHANICAL FASTENING DOCUMENT CCP-NEU-XXX.

NOTES: UNLESS OTHERWISE SPECIFIED

METRIC

THIRD ANGLE PROJECTION

DRILL HOLE SIZE	TOLERANCE
0.35 THRU 3.20	+0.10 / -0.03
3.21 THRU 6.40	+0.13 / -0.03
6.41 THRU 12.70	+0.15 / -0.05
12.71 THRU 19.00	+0.20 / -0.05
19.01 THRU 25.40	+0.25 / -0.08

UNLESS OTHERWISE SPECIFIED: DIMENSIONS ARE IN MILLIMETERS. TOLERANCES ARE:
X.X ±0.25 ANGLES: ± 0°- 30'
X.XX ±0.13 CHAMFERS: ±5°

MATERIAL

FINISH

DATE 2021-01-06
DRAWN G. TEICHMAN
CHECKED
DESIGN
APPROVED 2021-01-08

NEUtron DOSimetry & Exploration CubeSat Project
McMaster University

TITLE: HASP 2021 PAYLOAD FULL ASSEMBLY

SIZE B | DWG. NO. CCP-HSP21-001-AD | REV -

SCALE 1:2 | DO NOT SCALE DRAWING | SHEET 1 OF 2

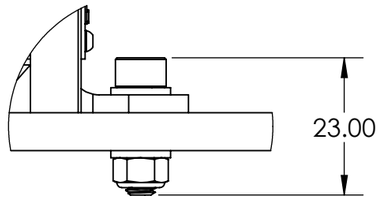

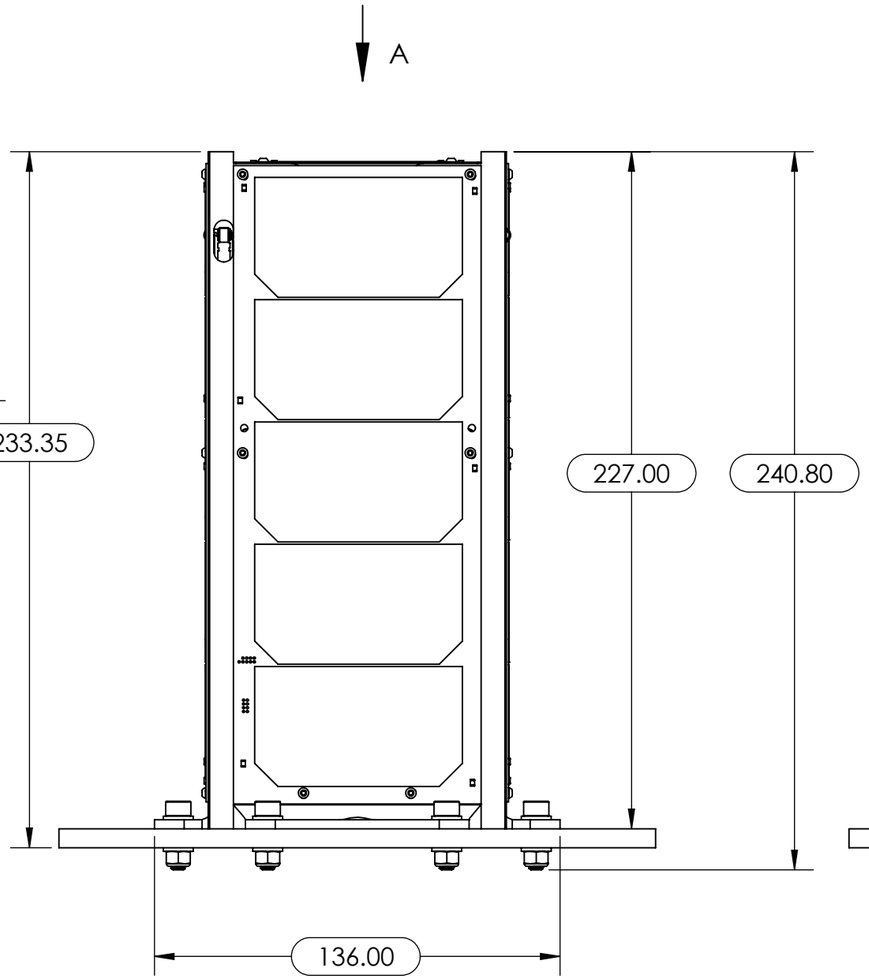

DETAIL B
SCALE 1 : 1

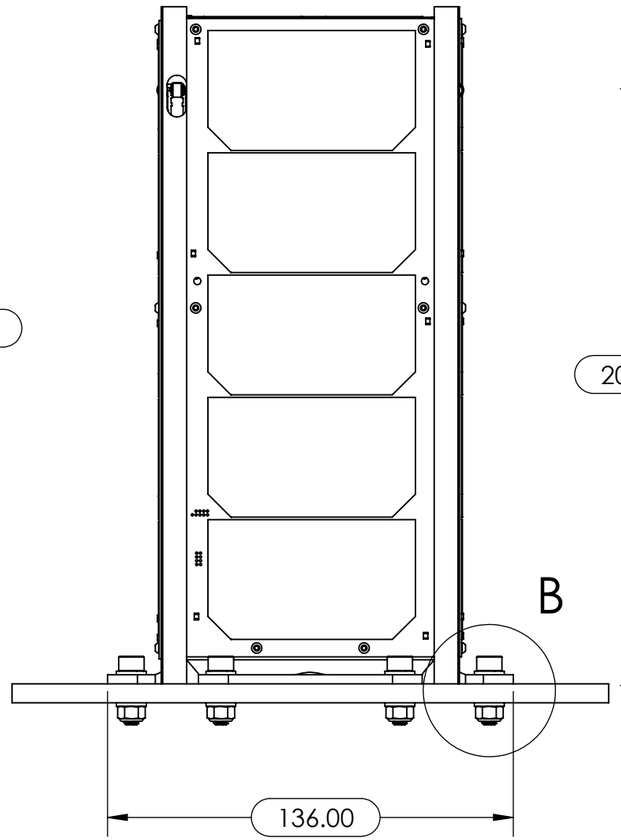

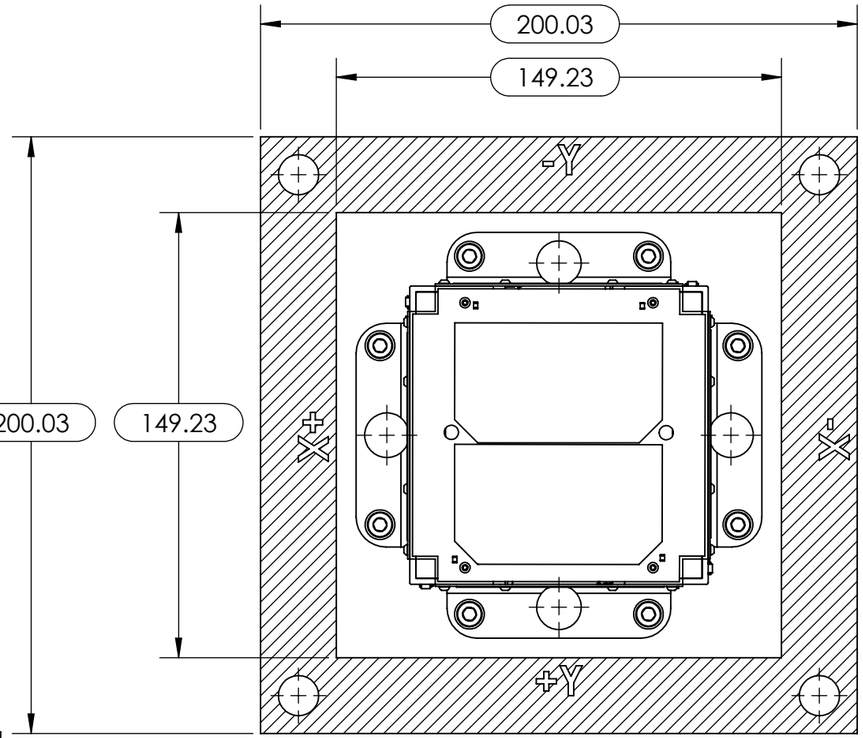

VIEW A

NEUtron DOSimetry & Exploration CubeSat Project McMaster University		
TITLE: HASP 2021 PAYLOAD FULL ASSEMBLY		
SIZE B	DWG. NO. CCP-HSP21-001-AD	REV -
SCALE 1:2	DO NOT SCALE DRAWING	SHEET 2 OF 2

REVISIONS				
ZONE	REV.	DESCRIPTION	DATE	APPROVED

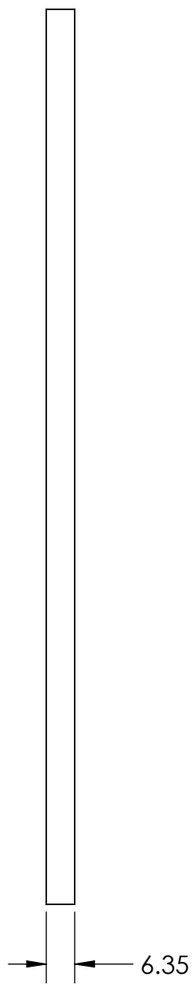

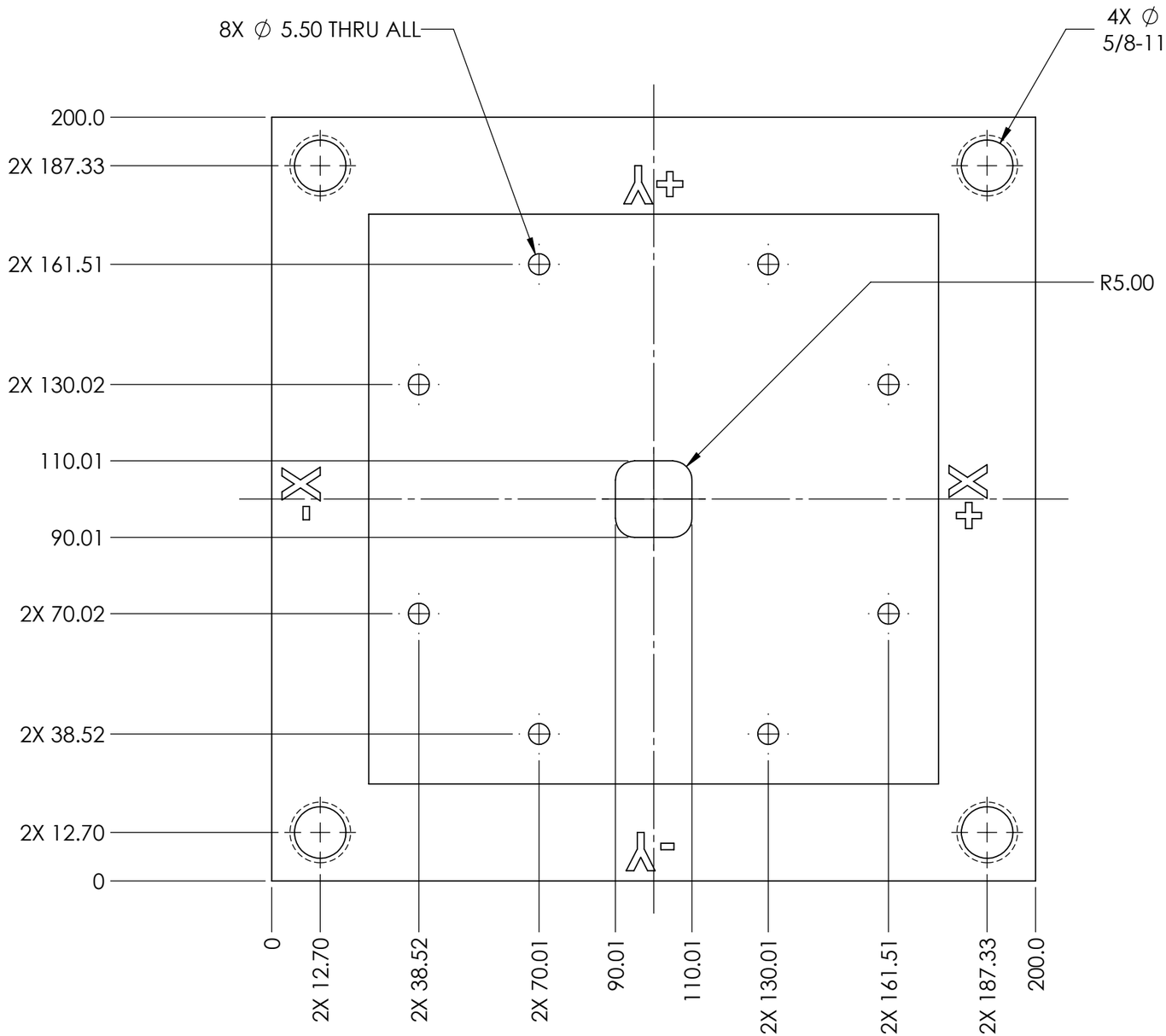

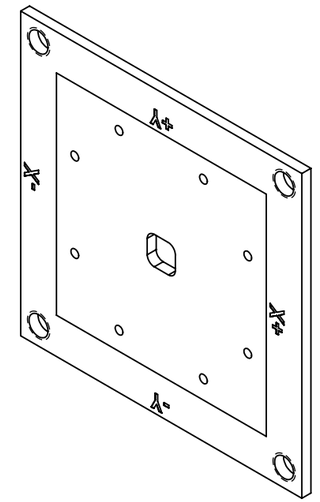

△3 FINISH: NONE

△2 MATERIAL: N/A

1. DIMENSIONAL LIMITS APPLY AFTER △3 .

NOTES:

METRIC

THIRD ANGLE PROJECTION	
DRILL HOLE SIZE	TOLERANCE
0.35 THRU 3.20	+0.10 / -0.03
3.21 THRU 6.40	+0.13 / -0.03
6.41 THRU 12.70	+0.15 / -0.05
12.71 THRU 19.00	+0.20 / -0.05
19.01 THRU 25.40	+0.25 / -0.08

UNLESS OTHERWISE SPECIFIED:
DIMENSIONS ARE IN MILLIMETERS.
TOLERANCES ARE:
X.X ±0.25 ANGLES: ± 0°- 30'
X.XX ±0.13 CHAMFERS: ±5°

MATERIAL △2

FINISH △3

DATE 12-16-2020

DRAWN J. ONESI

CHECKED

DESIGN

APPROVED

NEUtron DOSimetry & Exploration CubeSat Project
McMaster University

TITLE: HASP MOUNTING PLATE

SIZE **B** | DWG. NO. | REV -

SCALE 3:4 | DO NOT SCALE DRAWING | SHEET 1 OF 1

5. References

[1] Cucinotta, F. A. (2015). Review of NASA approach to space radiation risk assessments for Mars exploration. Health physics, 108(2), 131-142.
[2] Cucinotta, F. A., Schimmerling, W., Wilson, J. W., Peterson, L. E., Badhwar, G. D., Saganti, P. B., & Dicello, J. F. (2001). Space radiation cancer risks and uncertainties for Mars missions. Radiation research, 156(5), 682-688.
[3] Cucinotta, F. A., & Durante, M. (2006). Cancer risk from exposure to galactic cosmic rays: implications for space exploration by human beings. The lancet oncology, 7(5), 431-435.
[4] Dietze, G., Bartlett, D. T., Cool, D. A., Cucinotta, F. A., Jia, X., McAulay, I. R., ... & Sato, T. (2013). Icrp publication 123: Assessment of radiation exposure of astronauts in space. Annals of the ICRP, 42(4), 1-339.
[5] United States. National Aeronautics and Space Administration. Office of Inspector General. (2011). A review of NASA's replacement of radiation monitoring equipment on the International Space Station. [Washington, D.C.]: Office of Audits, Office of Inspector General, National Aeronautics and Space Administration.
[6] Glenn, V. D. (2006). NTRS: NASA Technical Reports Server. Reference Reviews.
[7] Armstrong T, Colborn B. Predictions of secondary neutrons and their importance to radiation effects inside the international space station. Radiat Meas 2001; 33:229–34.
[8] Badhwar, G. D., Keith, J. E., & Cleghorn, T. F. (2001). Neutron measurements onboard the space shuttle. Radiation measurements, 33(3), 235–241.
[9] Hanu, A. R., Barberiz, J., Bonneville, D., Byun, S. H., Chen, L., Ciambella, C., ... & Jhirad, A. (2017). NEUDOSE: A CubeSat Mission for Dosimetry of Charged Particles and Neutrons in Low-Earth Orbit. Radiation research, 187(1), 42-49.
[10] E. R. Benton and E. V. Benton, “Space radiation dosimetry in low-Earth orbit and beyond,” Nucl. Instruments Methods Phys. Res. Sect. B Beam Interact. with Mater. Atoms, vol. 184, no. 1–2, pp. 255–294, 2001.
[11] Schröder, F. G. (2017). Radio detection of cosmic-ray air showers and high-energy neutrinos. Progress in Particle and Nuclear Physics, 93, 1-68.
[12] Goldhagen, P., Reginatto, M., Kniss, T., Wilson, J. W., Singleterry, R. C., Jones, I. W., & Van Steveninck, W. (2002). Measurement of the energy spectrum of cosmic-ray induced neutrons aboard an ER-2 high-altitude airplane. Nuclear Instruments and Methods in Physics Research Section A: Accelerators, Spectrometers, Detectors and Associated Equipment, 476(1-2), 42-51.
[13] Poje, M., Vukovic, B., Radolic, V., Miklavcic, I., & Planinic, J. (2015). Neutron radiation measurements on several international flights. Health physics, 108(3), 344-350.
[14] Cecchetto, M., García Alía, R., & Wrobel, F. (2019). Impact of Energy Dependence on Ground Level and Avionic SEE Rate Prediction When Applying Standard Test Procedures. Aerospace, 6(11), 119.
[15] T. Sato. EXPACS: Excel-based Program for calculating Atmospheric Cosmic-Ray Spectrum. UserâAZs Manual. 2009.

Appendix A: Timeline and Milestone WBS Documentation

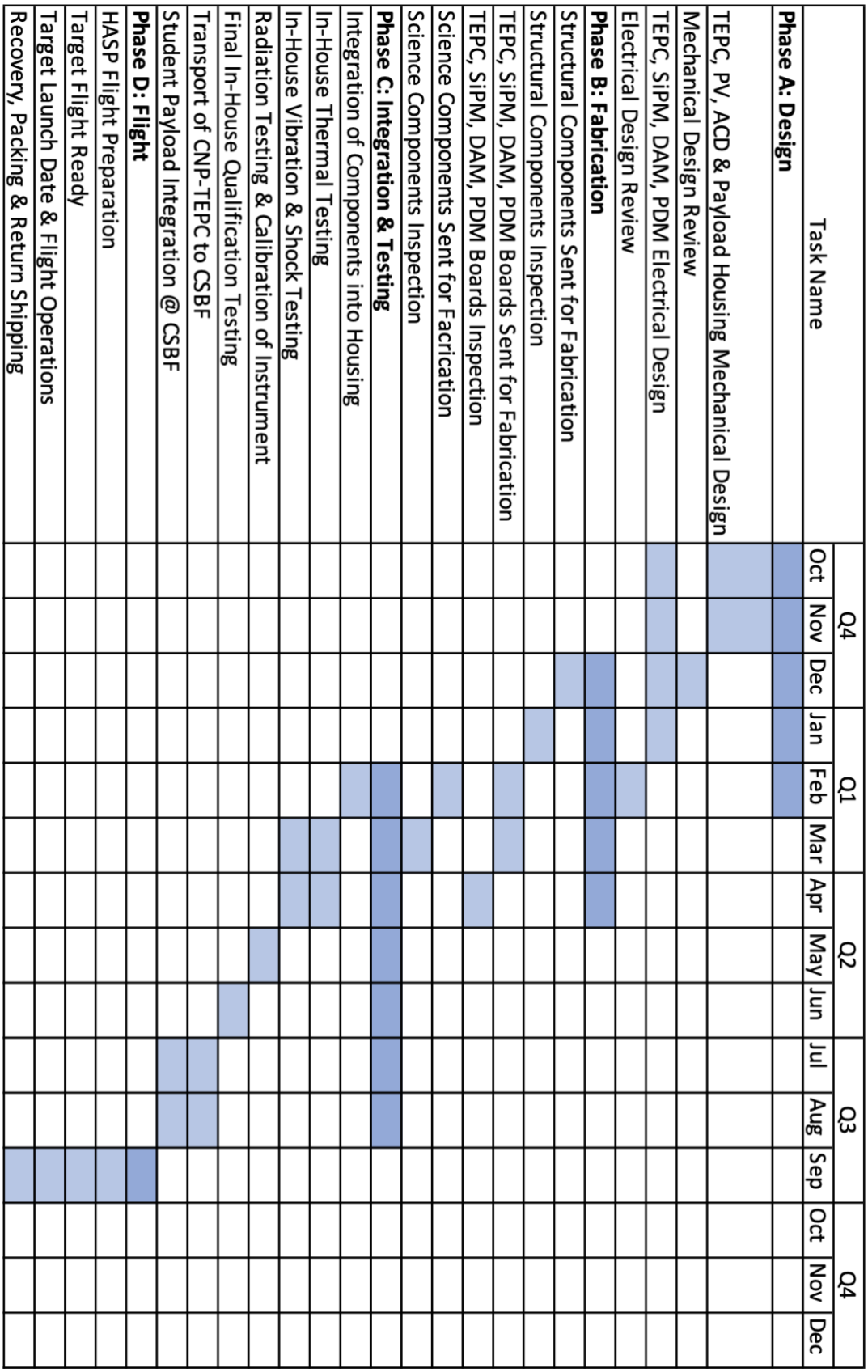

Figure 17: Detailed gantt chart displaying the projected schedule for the CNP-TEPC leading up to HASP 2021.

Appendix B: Existing Components

Figure 18: HASP 2017 Payload from McMaster NEUDOSE.

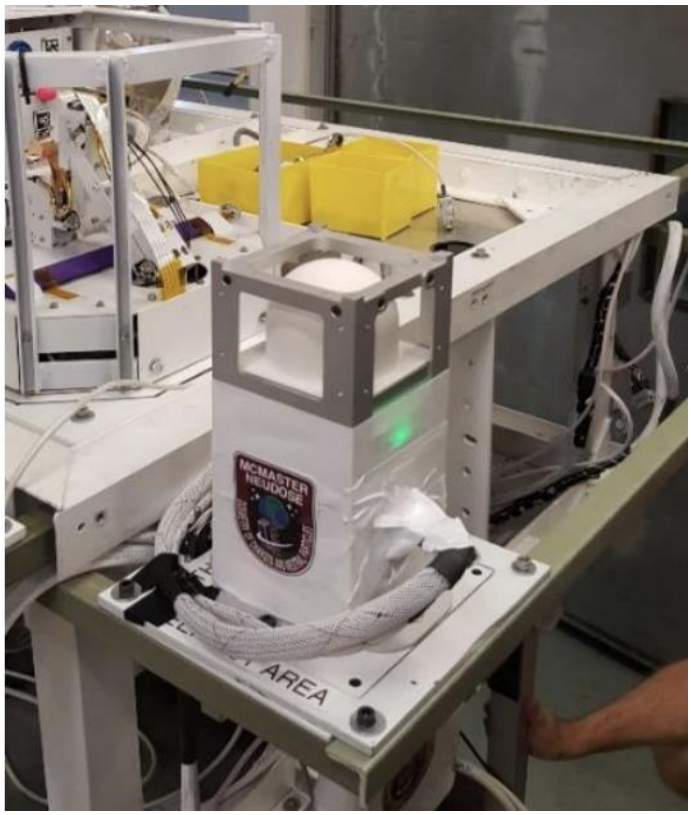

Figure 19: HASP 2018 Payload from McMaster NEUDOSE.

Figure 20: Undercut (left) and overcut (right) hemispheres to make the TE sphere, fabricated in March 2019.

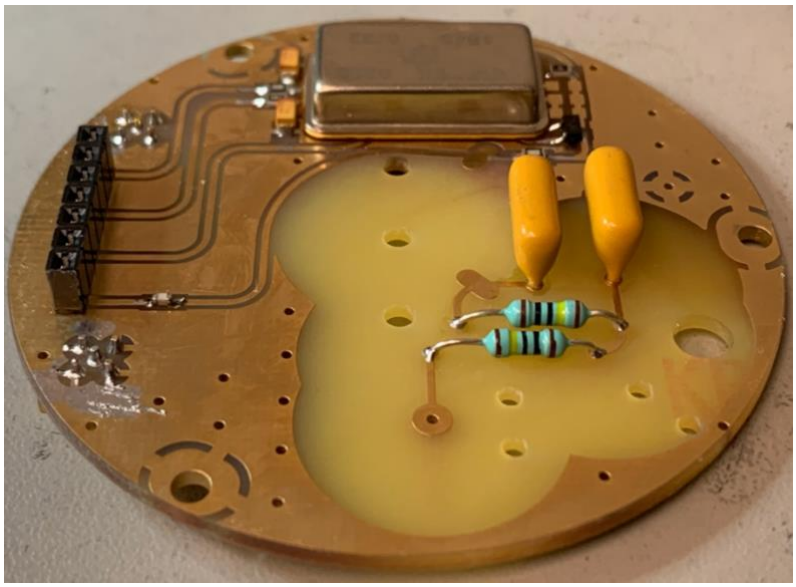

Figure 21: PCB bottom view of the Preamplifier Module, fabricated January 2020.

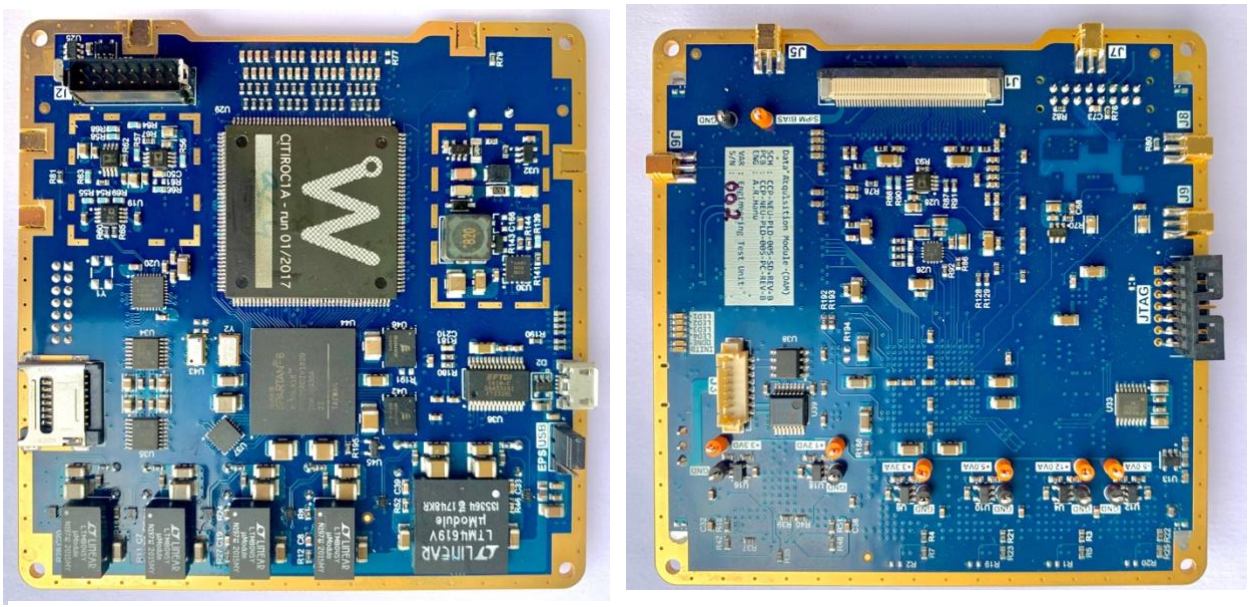

Figure 23: PCB top view (left) and bottom view (right) of the DAM, fabricated December 2020.

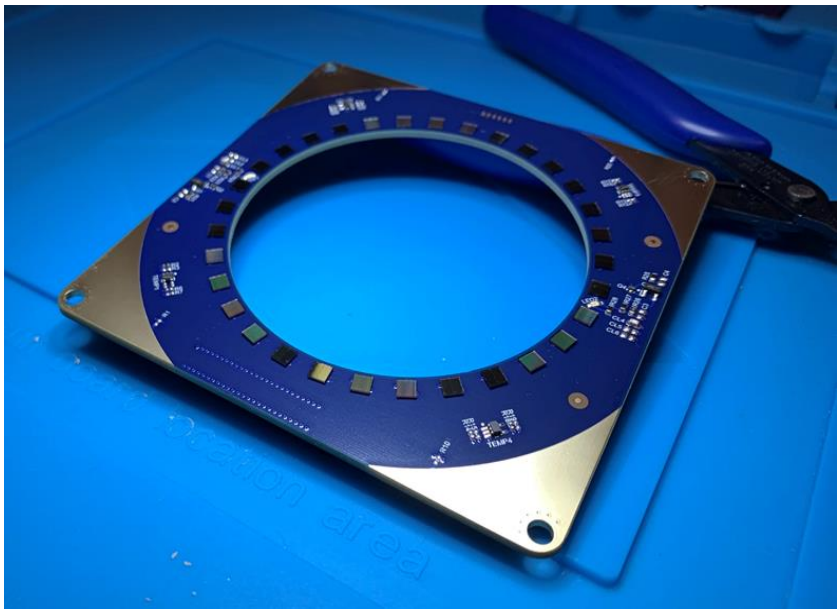

Figure 22: PCB top view of the SiPM Module. Manufactured in October 2020.

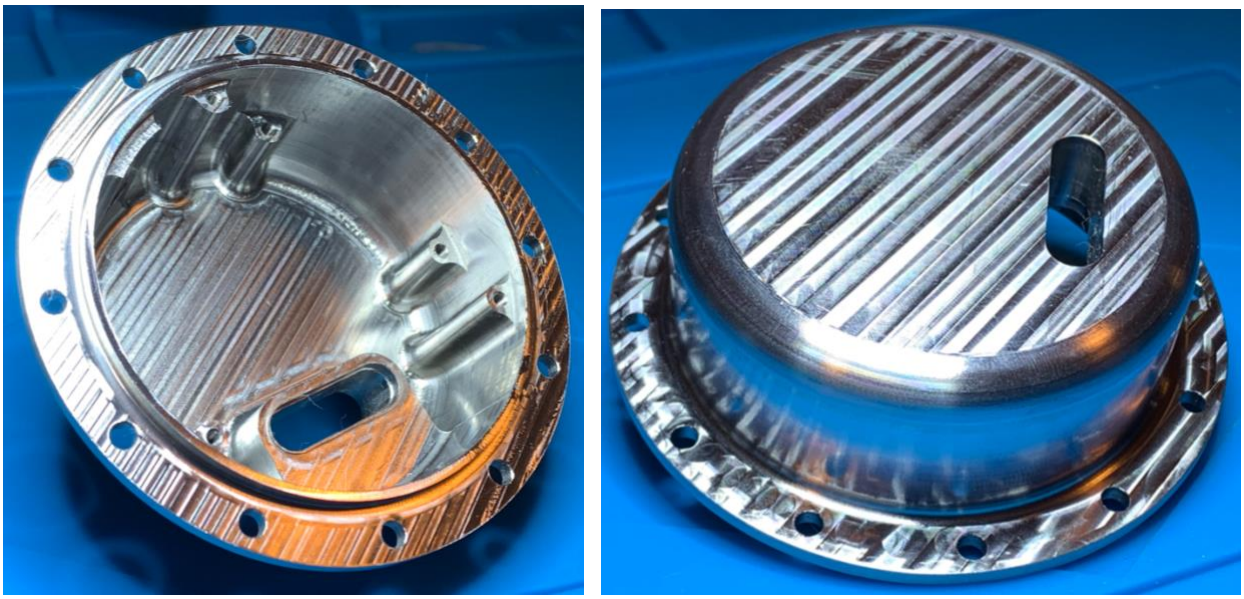

Figure 25: Payload detector vessel base top view (left) and bottom view (right), fabricated November 2020.

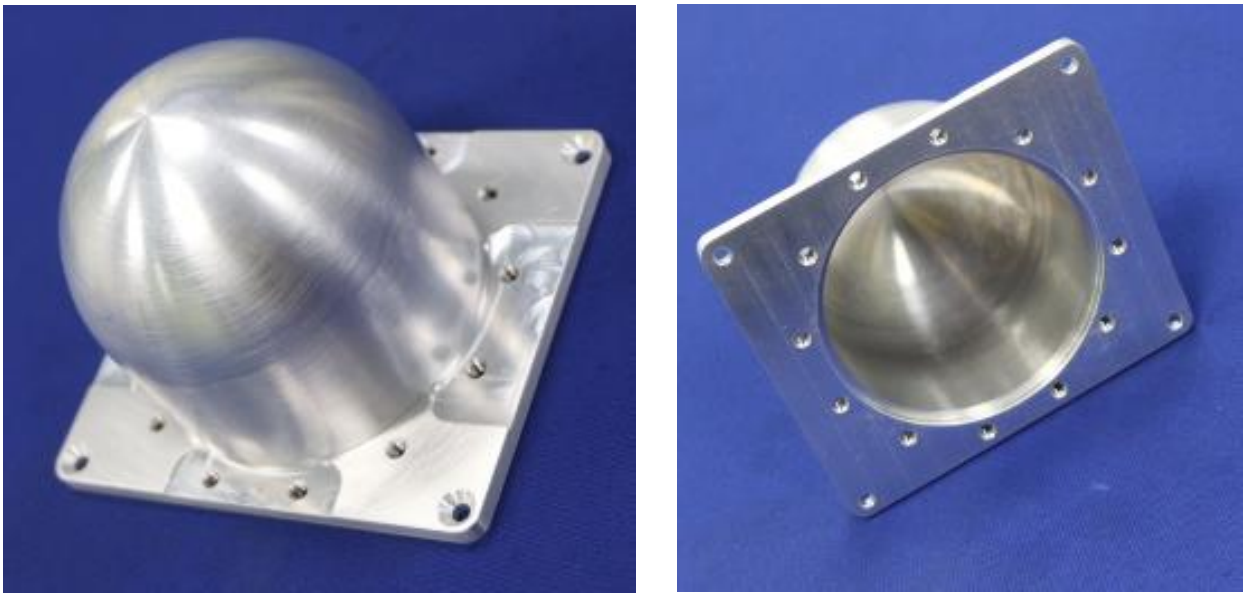

Figure 24: Payload detector vessel lid top view (left) and bottom view (right), fabricated December 2020.

Figure 27: Scintillators manufactured in December 2020. Scintillators were manufactured with (right) and without (left) polishing and a reflective paint coating to determine which will show better performance.

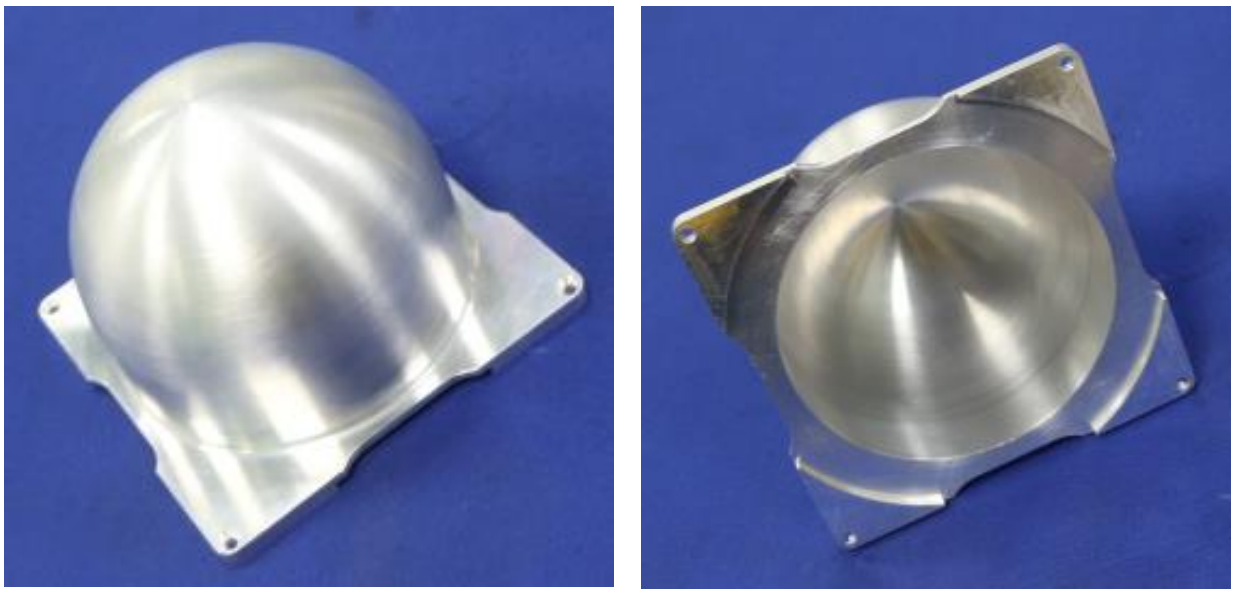

Figure 26: Payload ACD Lid top view (left) and bottom view (right), fabricated December 2020.

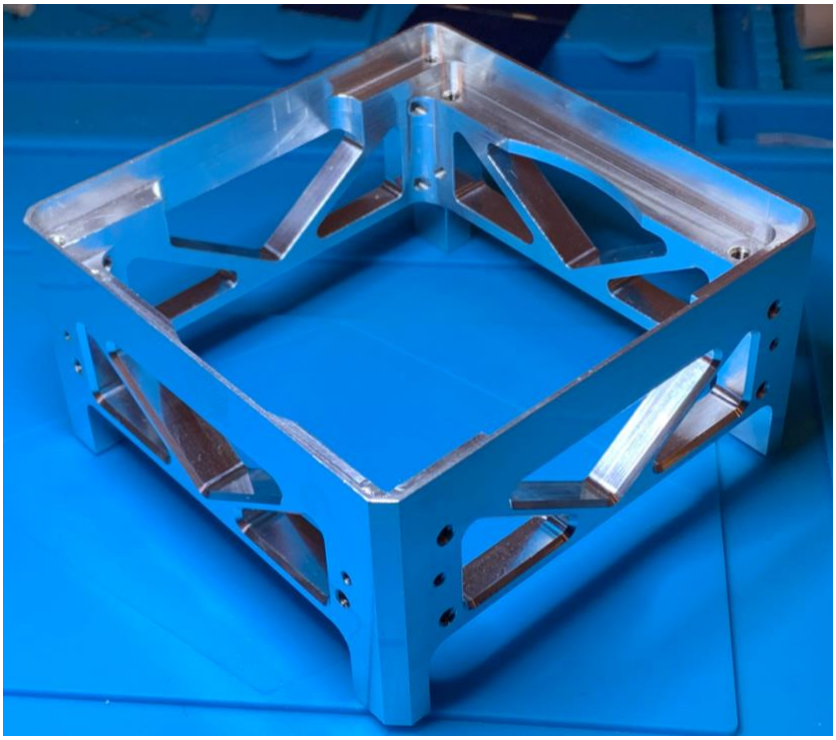

Figure 28: Payload housing fabricated in November 2020.

Appendix C: Packet Structure

Table 5: Serial data structure of housekeeping data.

Byte(s)	Hex Value	Running Total	Description
Header			
8	0x50 41 59 4C 4F 41 44 21	8	Start of Packet
1	0x00	9	Packet ID
1		10	Version Number
5		15	Data Length
Data			
2	0x25 48	17	Start of Housekeeping Data
4		21	Live time (centiseconds)
4		25	Deadtime correction counter 1
4		29	Deadtime correction counter 2
2		31	TEPC Pressure (100 x torr)
2		33	TEPC Threshold (10 x V)
2		35	SiPM High Voltage (100 x V)
125		160	GPS String (Start of Acquisition)
125		285	GPS String (End of Acquisition)
2		287	ADC1_3: 12V Supply Current Monitor
2		289	ADC1_4: +5V Supply Current Monitor
2		291	ADC1_5: +5V Supply Voltage Monitor
2		293	ADC1_6: 3.3V Analog Current Monitor
2		295	ADC1_7: 3.3V Analog Voltage Monitor
2		297	ADC2_0: 3.3V Digital Current Monitor
2		299	ADC2_1: 3.3V Digital Voltage Monitor
2		301	ADC2_2: 1.2V Supply Current Monitor
2		303	ADC2_3: 1.2V Supply Voltage Monitor
2		305	ADC2_4: VBUS Current Monitor
2		307	ADC2_5: VBUS Voltage Monitor
2		309	ADC2_0: SiPM Bias Voltage Monitor
2		311	ADC2_1: SiPM Bias Current Monitor
2		313	ADC2_2: CITIROC Temperature
2		315	ADC2_3: SiPM Surface Temperature Sensor 2 (100 x K)
2		317	ADC2_4: SiPM Surface Temperature Sensor 1 (100 x K)
2		319	ADC2_5: SiPM Surface Temperature Sensor 4 (100 x K)
2		321	ADC2_6: SiPM Surface Temperature Sensor 3 (100 x K)
2		323	ADC2_7: TEPC High Voltage Power Supply Voltage Monitor (10 x V)

Footer			
2	0x25 58	325	End of Packet
1		326	XOR Redundancy check

Table 6: Serial data structure of histogram data.

Byte(s)	Hex Value	Running Total	Description
Header			
8	0x50 41 59 4C 4F 41 44 21	8	Start of Packet
1	0x00	9	Packet ID
1		10	Version Number
5		15	Data Length
Data			
2	0x2547	17	Start of Histogram Data
4		21	Live time (centiseconds)
4		25	Deadtime correction counter 1
4		29	Deadtime correction counter 2
2		31	TEPC Pressure (100 x torr)
2		33	TEPC Threshold (10 x V)
2		35	SiPM High Voltage (100 x V)
2		37	SiPM Threshold (100 x V)
2		39	Number of bins (0-16384 possible bins)
2	0x25 41	41	Start of Anti-coincidence spectrum data
2		43	ACOINC bin 0 counts
2		45	ACOINC bin 1 counts
...	...	...	...
2		32807	ACOINC bin 16382 counts
2		32809	ACOINC bin 16383 counts
2	0x25 43	32811	Start of Coincidence spectrum data
2		32813	COINC bin 0 counts
2		32815	COINC bin 1 counts
...	...	...	...
2		65577	COINC bin 16382 counts
2		65579	COINC bin 16383 counts
Footer			
2	0x25 58	65581	End of Packet
1		65582	XOR Redundancy check

Appendix D: Detector Vessel Stress Analysis and Construction

The detector vessel's fill pressure is between 30 and 40 torr, much lower than that of standard atmospheric pressures. As a result, the net forces acting on the detector vessel are greatest at ground level atmospheric conditions. An FEA study was conducted to determine how these stresses will act on the detector vessel under worst case operating conditions.

Figures 28 to 37 show the results of a static study assuming an atmospheric pressure of 104.8 kPa with a pure vacuum inside the detector. This state represents the absolute peak loading anticipated on the detector vessel during backfilling of the vessel with TE gas. A bonded contact set between the upper and lower detector halves was used and a 104.8 kPa pressure load was applied on all exterior faces as well as the inner bulkhead assuming improper contact of the micro-D connector. The vessel was constrained using the 4 mounting holes on the upper lid.

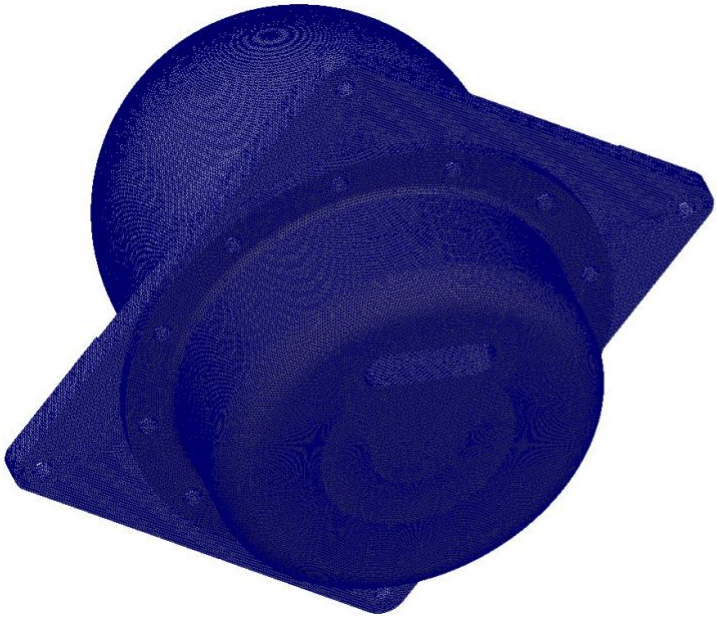

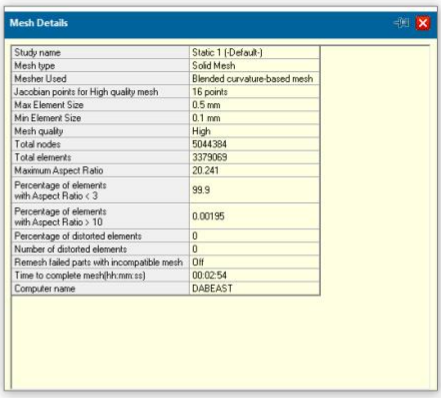

Figure 29: Mesh used for study: 3,379,069 solid 3D elements with 99.9% elements having an aspect ratio less than 3. 0.5mm average element size to capture thin wall features.

Load Case 1: Internal Vacuum Prior to Backfilling

Due to the geometry of the detector vessel, the domed upper half of the vessel sees relatively little stress under atmospheric loading conditions compared to the vessel base. Due to the flat bottom of the detector base, larger stresses are seen on the bottom side of the detector, on average of 32 MPa as seen in the figures below.

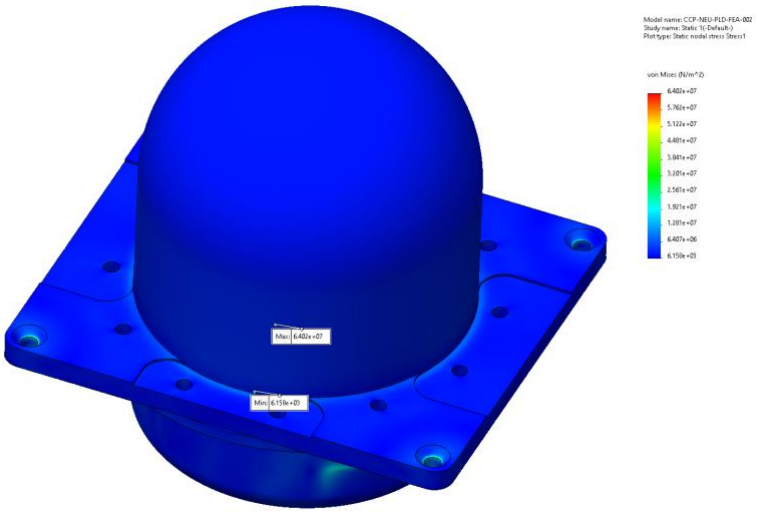

Figure 30: von Mises Stress results, 104.8 kPa atmospheric load, vacuum inside detector.

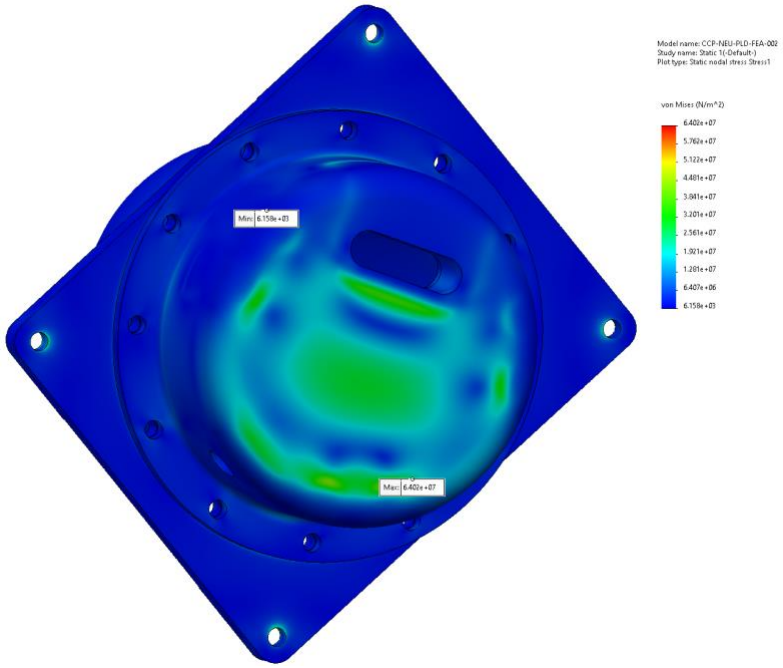

Figure 31: von Mises Stress results on exterior face, 104.8 kPa atmospheric load, vacuum inside detector.

The peak stress seen in the detector vessel under these loading conditions are found inside the detector vessel base. Transition radii between board standoffs and the bottom of the base create slight stress risers causing stress peaks in these regions as seen in the below figure. However even the latest peak stress seen of 64 MPa gives the detector vessel a FOS of 3.3 based on this loading scenario. During normal operation, this safety factor will be slightly higher as the TE gas fill pressure will reduce the net pressures acting on the detector vessel.

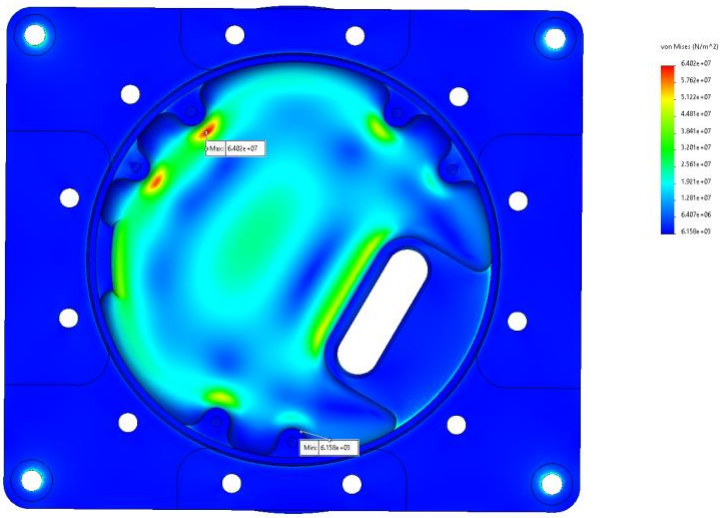

Figure 32: von Mises Stress results interior face, 104.8 kPa atmospheric load, vacuum inside detector, peak stress of 64 MPa in transition region of board standoff on vessel base.

Load Case 2: Pressurized Vessel in External Vacuum

A similar simulation was conducted assuming a pure vacuum environment and a 40 torr fill pressure within the detector vessel. This is representative of the TEPC's expected operating environment. The same mesh and fixtures were used as before with a 40 torr pressure applied to all inner faces of the vessel.

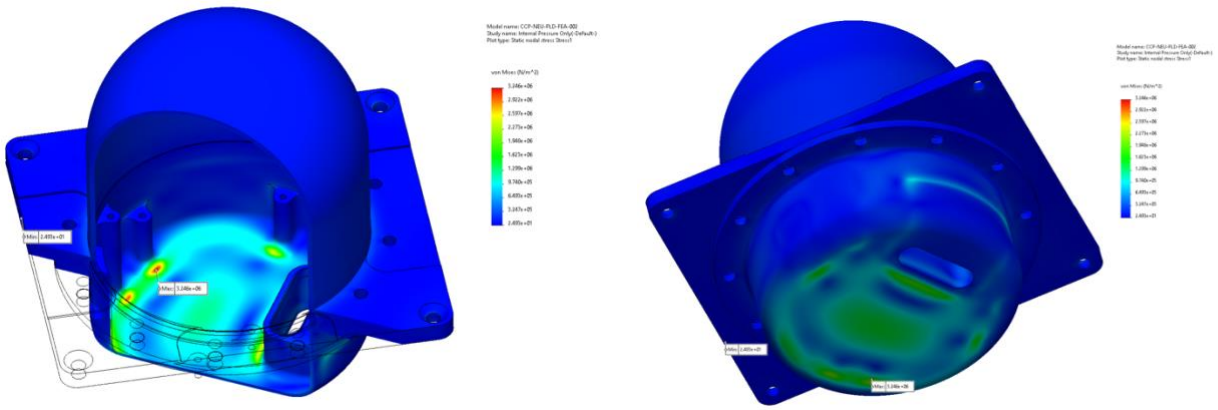

a. b.

Figure 33: a. von Mises Stress results: 40 torr (5332.89 Pa) internal pressure. Peak stress 3.25 MPa. b. von Mises Stress results: 40 torr (5332.89 Pa) internal pressure. View of external bottom.

This load case is much smaller than the first case (5.3 kPa load compared to 104 kPa) and as expected, the peak stress occurs again in the transition region of the vessel base. However, with such a low stress, the factor of safety in this case is a minimum of 64.

Linear Buckling Analysis

In addition to a static load analysis on the detector vessel, an eigenvalue linear buckling analysis was performed to investigate other failure modes besides static yielding. The below figures illustrate the first four modes with positive load factors acting on the detector vessel.

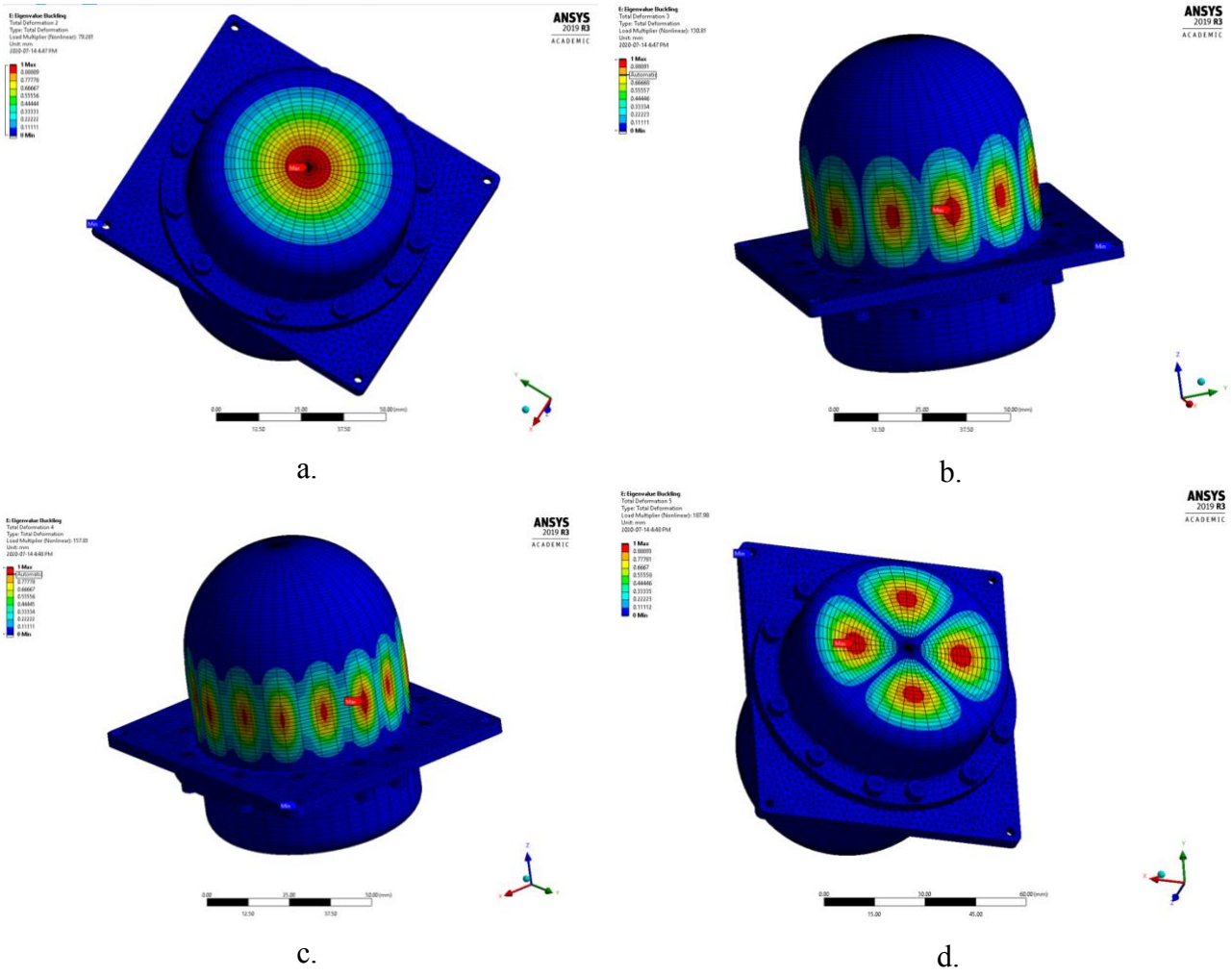

Figure 34: a. Eigenvalue buckling Results: Mode 1, Load factor: 79.2. b. Eigenvalue buckling Results Mode 2, Load factor: 130.8. c. Eigenvalue buckling Results Mode 3, Load factor: 157.8. d. Eigenvalue buckling Results Mode 4, Load factor: 188.0.

With a first mode load factor of 79 and the worst case loading of the detector vessel in atmospheric conditions, we do not expect a failure of the detector vessel through buckling of the vessel walls.

Appendix E: DAM Communication and Memory Information

Communication

The DAM uses several different communication standards to communicate the information acquired from each section of the PCB. The main communication standard between all areas on the board is communicated with the Serial Peripheral Interface (SPI) protocol. The DAM houses several different ICs to convert the inputted SPI communication into a different communication standard based on what the information is interfacing with.

SPI

FPGA ↔ CAN-Controller ↔ CAN Transceiver ↔ PDM Connector
FPGA ← Housekeeping ADC 1
FPGA ← Housekeeping ADC 2
FPGA ← Housekeeping ADC 3
FPGA → DAC-Front End Adjust → Analog Front End
FPGA → DAC-HVPS Adjust → PV Connector
FPGA ← CITIROC ADC
FPGA ↔ MRAM

RS232

FPGA ↔ UART ↔ RS232 Transceiver ↔ PDM Connector

Memory

Within the DAM, there are several different types of memory that are used. Within the FPGA, there is the Block RAM, used to store information from one section of the FPGA to another. There is also MRAM on the DAM, a non-volatile type of memory used to store acquired science information. Lastly there is SD Flash Memory, which is used for on ground testing information.

BRAM Memory
Within the DAM, there are several different types of memory that are used. Within the FPGA, there is the Block RAM, used to store information from one section of the FPGA to another. There is also MRAM on the DAM, a non-volatile type of memory used to store acquired science information. Lastly there is SD Flash Memory, which is used for on ground testing information.

MRAM Memory
The DAM has a single block of non-volatile MRAM to store acquired science information. This Magneto-resistive RAM stores data within magnetic domains, while also maintaining a level of magneto-resistive qualities. The MRAM memory has a 4 MB capacity, able to store 8 bits of data through 24 different address bits. The memory is transferred to and from the FPGA in the SPI format.

MicroSD Flash Memory

The SD Memory is a form of non-volatile memory that is used to store science data. This microSD card memory can be used for both ground testing or in this case, for the HASP 2021 mission to collect acquired data as well as flight data. The memory suggested to be used is a 2 GB card. For HASP 2021, a microSD card will be used in parallel with the RS232 communication in order to keep a record of all communication with the ground throughout the duration of the payload's flight.